



Original article

Photochemical electrocyclisation of 3-vinylindoles to pyrido[2,3-*a*]-, pyrido[4,3-*a*]- and thieno[2,3-*a*]-carbazoles: Design, synthesis, DNA binding and antitumor cell cytotoxicity

Thomas Lemster^{a,*}, Ulf Pindur^a, Gaëlle Lenglet^{b,c}, Sabine Depauw^{b,c}, Christelle Dassi^{b,c}, Marie-Hélène David-Cordonnier^{b,c,**}

^a Institute of Pharmacy, Department of Pharmaceutical and Medicinal Chemistry, Johannes Gutenberg-University, Staudingerweg 5, D-55099 Mainz, Rheinland-Pfalz, Germany

^b INSERM U837-JPARC (Jean-Pierre Aubert Research Center), Team "Molecular and Cellular Targeting for Cancer Treatment", Institut de Recherches sur le Cancer de Lille, Place de Verdun, F 59045 Lille Cedex, France

^c Université de Lille 2, IMPRT-Institut Fédératif de Recherche 114, Lille, France

ARTICLE INFO

Article history:

Received 17 October 2008

Received in revised form

13 March 2009

Accepted 19 March 2009

Available online 27 March 2009

Keywords:

DNA ligands

Pyridocarbazoles

DNA intercalation

DNA minor groove binding

ABSTRACT

In the context of the design and synthesis of DNA ligands, some new hetarene annelated carbazoles were synthesized. As lead structure the intercalating tetracyclic systems pyrido[2,3-*a*]- and pyrido[4,3-*a*]-carbazoles and in one case a thieno[2,3-*a*]-carbazole were taken into account. A dialkyl amino amidic chain was introduced to the planar chromophoric system with the intent to generate minor groove binding properties. The cytotoxicity of some compounds was examined by the NCI antitumor screening. Furthermore, biophysical as well as biochemical studies were performed in order to get some information about the DNA-binding properties and inhibition of DNA related functional enzymes of this new series of molecules.

Crown Copyright © 2009 Published by Elsevier Masson SAS. All rights reserved.

1. Introduction

Since the discovery of the natural products ellipticine **1** and its regioisomeric olivacine **2** annelated indole and carbazole derivatives with pyrido[4,3-*b*]carbazole framework constitute an interesting class of antitumor active drugs [1–4]. Whereas ellipticine **1** as well as 9-methoxyellipticine **3** shows activity against a variety of human tumor cell lines, especially against leukaemia, the quaternary pyridinium salt ellipticinium acetate (Celliptium®) **4** was deployed against metastatic breast cancer [3,5]. The mechanism of action *in vivo* of ellipticine and variants via DNA-intercalation process, bioactivation due to oxidation at C-9 and indirect topoisomerase II-inhibition is well described [4,6]. In this context many derivatives based on the linear annelated carbazole ellipticine and olivacine were synthesized for the development of new DNA-intercalating anticancer drugs [2,3,7]. However, only a few studies

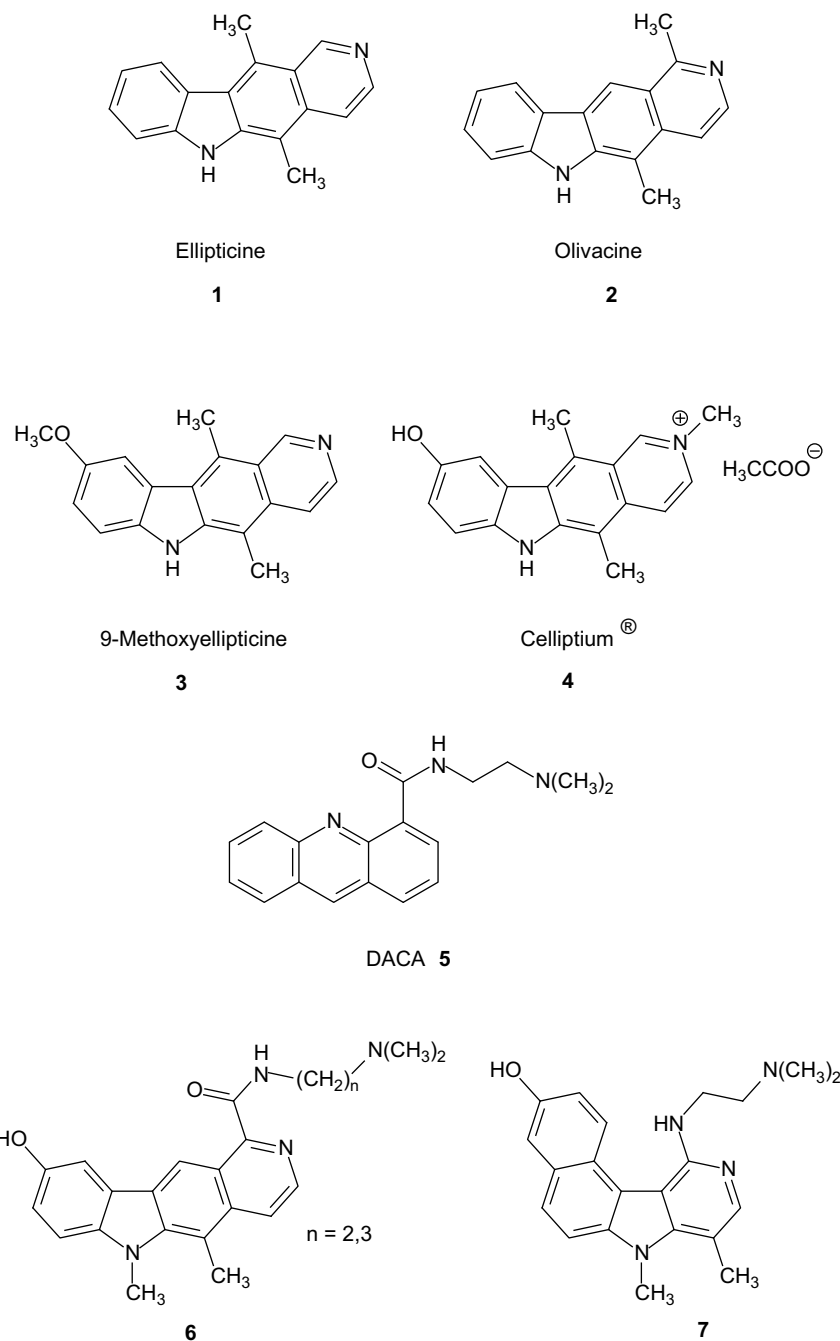
were carried out with compounds bearing an angled pyridocarbazole annelation [6,11]. Thus, in continuation of our synthetic efforts in carbazole and carbazole alkaloid chemistry [12,13], we studied new short and flexible routes to some hetarene-[*a*]-annelated carbazoles of type **10**. Moreover, derived from some literature reports [3,7,14] and from our own results in the netropsin series [15–19], the selective introduction of a dimethylaminoalkyl-carboxamide group at the coplanar chromophoric system should be of significant importance for a selective DNA binding and antitumor activity. For example DACA (*N*-[2-(dimethylamino)-ethyl]-acridine-4-carboxamide) **5** is a dual topoisomerase I/II inhibitor and DNA intercalator with potent cytotoxicity against leukaemia cell lines. Its carboxamide group is essential to the biological activity [14]. The olivacine derivatives **6** (*n* = 2: S16020-2) and the γ -carboline **7** are further examples of drugs which bear a dimethylaminoalkylamino functionality as an important DNA-binding structure element which increases the cytotoxicity and antitumor activity (Scheme 1) [3,7–10].

On the background of these findings we describe in the present paper the preparation of new pyrido- and thieno-[*a*]-annelated carbazoles **10** bearing a dimethylaminoalkyl-carboxamide moiety at the carbazole ring C. In one case a morpholino moiety as cyclic

* Corresponding author.

** Corresponding author.

E-mail addresses: lemster@uni-mainz.de (T. Lemster), marie-helene.david@inserm.fr (M.-H. David-Cordonnier).



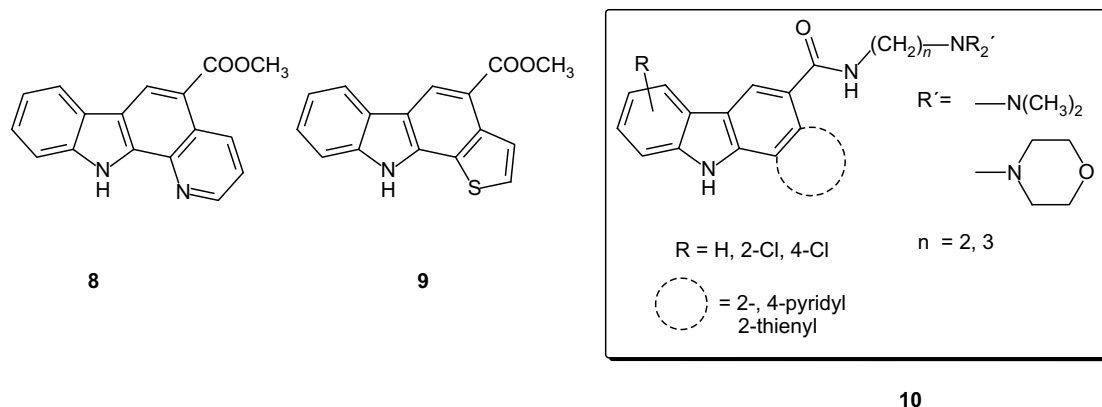
Scheme 1. Lead compounds: examples of annelated N-heterocycles as intercalating antitumor active drugs.

structural element was introduced. These products can be considered formally as regioisomeric and/or bioisosteric ellipticine derivatives combining an appropriate carboxamide structural element. The synthetical key step comprises a photochemically induced 6π -electrocyclisation, a convenient procedure derived from synthetic developments in our group [13,20]. For the establishment of primary structure–activity relationships (DNA-binding cytotoxicity) of these new functionalised carbazoles some biophysical, biochemical and cell biological studies were performed.

2. Chemistry

In former studies in our group, the synthesis of new benzo[*a*]-annelated carbazoles via photochemically induced

6π -electrocyclisation of 2-phenyl-3-vinylindoles has been established [20]. This convenient method has now been transferred to produce new pyrido- and thieno[*a*]carbazoles **8**, **9** as chromophoric systems starting from the corresponding 2-hetarene-3-methylacrylate substituted indoles. Preorientating ΔT_m -value measurements of basic compounds **8** and **9** [18–20] exhibit no DNA binding at all. Thus, in relation to compounds **5–7** an amidic chain as potential binding element into the minor groove of DNA has been introduced (**10**) (Scheme 2). As already described above, a dimethylamino-ethylamino- and the homologue dimethylamino-propylamino-function approved to have an optimal distance between the conjugated π -system and the tertiary aliphatic nitrogen as potential H-bond acceptor. Moreover the basic substituted carboxamide function comprises additional DNA-binding element (groove binding).



Scheme 2. Frameworks of the synthesized compounds (**8**, **9**), general formula of the [a]-annelated carbazole amides (**10**).

The access to the new compounds **10** is displayed exemplarily in Scheme 3. The synthetic sequence starts with the synthesis of the corresponding hydrazones **13** readily available from the reaction of phenylhydrazines **11** with 2- and 4-acetylpyridine **12** in very good yields. Subsequent Fischer cyclization of **13** gave rise to indoles **14** in the presence of polyphosphoric acid in all cases. The obtained indoles were formylated according to Vilsmeier–Haack reaction using phosphoryl chloride in DMF. The resulting carboxaldehydes **15** were converted stereoselectively into the (*E*)-methylacrylates **16** via Wittig reaction in good yield (46–76%). In the following key step reaction the 2-hetaryl-3-vinylindoles **16** were submitted to ultra-violet irradiation ($\lambda = 200\text{--}600\text{ nm}$) for a period of 4–8 h achieving directly the desirable [a]-annelated carbazole derivatives **17** via 6 π -electrocyclisation and subsequent dehydrogenation. Standard hydrolysis in 20% aqueous sodium hydroxide/ethanol gave rise to the carboxylic acid **18** completely. In the last step the introduction of the dimethylaminoalkyl linker succeeded by reaction of the free acid **18** with *N,N*-dimethylalkylene diamine in DMF with EDCI/HOBT as catalysts (Scheme 3). The amides **19** were obtained in good yields. Thus, for fine tuning developments and for establishing structure–activity relationships (DNA binding, topoisomerases inhibition, cytotoxicity) structural variations were performed. In one case the tertiary amine function was implemented in morpholine ring system (**29**).

The chloro derivatives **22–27** were synthesized in order to evaluate the influence of increased polar hydrophobicity and decreased density of electrons in the chromophoric structure. Moreover the exchange of the pyridine ring against a more lipophilic and more π -electron rich thiophene ring (see compound **28** in Table 1) should expand the spectrum of structure–activity relationship. Furthermore in the planar system the position isomeric pyrido[4,3-*a*]carbazoles **24**, **25** with a localized more peripheral nitrogen atom in the planar system were synthesized. These compounds should expand the activity pattern in comparison to the more lipophilic pyrido[2,3-*a*]carbazoles **20–23** relating to their biological/biophysical activities. The studies with the thiophene derivative **28** on DNA binding and topoisomerase inhibition demonstrated no significant advantage in comparison to the pyrido-derivatives, thus in the thiophene series no further synthetic variations were pursued so far (Table 1).

3. Biological and biophysical/biochemical methods

3.1. Cytotoxicity measurements

Due to restrictive criteria only three pyridocarbazole carboxamides were selected so far by the US National Cancer Institute [21] for evaluation in the in vitro preclinical antitumor screening

program against 60 human tumor cell lines. In the main screening, the sixty human tumor cell lines derived from the nine cancer types, leukaemia, non-small cell lung cancer, colon cancer, CNS cancer, melanoma, ovarian cancer, renal cancer, prostate cancer and breast cancer were used. The compounds' dose–response curves for each cell line were measured at a minimum of five concentrations at 10-fold dilutions in a protocol of 48 h continuous drug exposure, and a sulforhodamine B (SRB) protein assay was used to estimate cell viability or growth. The concentration causing 50% cell growth inhibition (GI_{50}), total cell growth inhibition (TGI, 0% growth) and 50% cell death (LC_{50} , –50% growth) compared with the control was calculated. In general, $\log_{10} GI_{50}$ values (the molar concentration of the drug resulting in inhibition of cell growth to 50% of control) were used for comparative discussion.

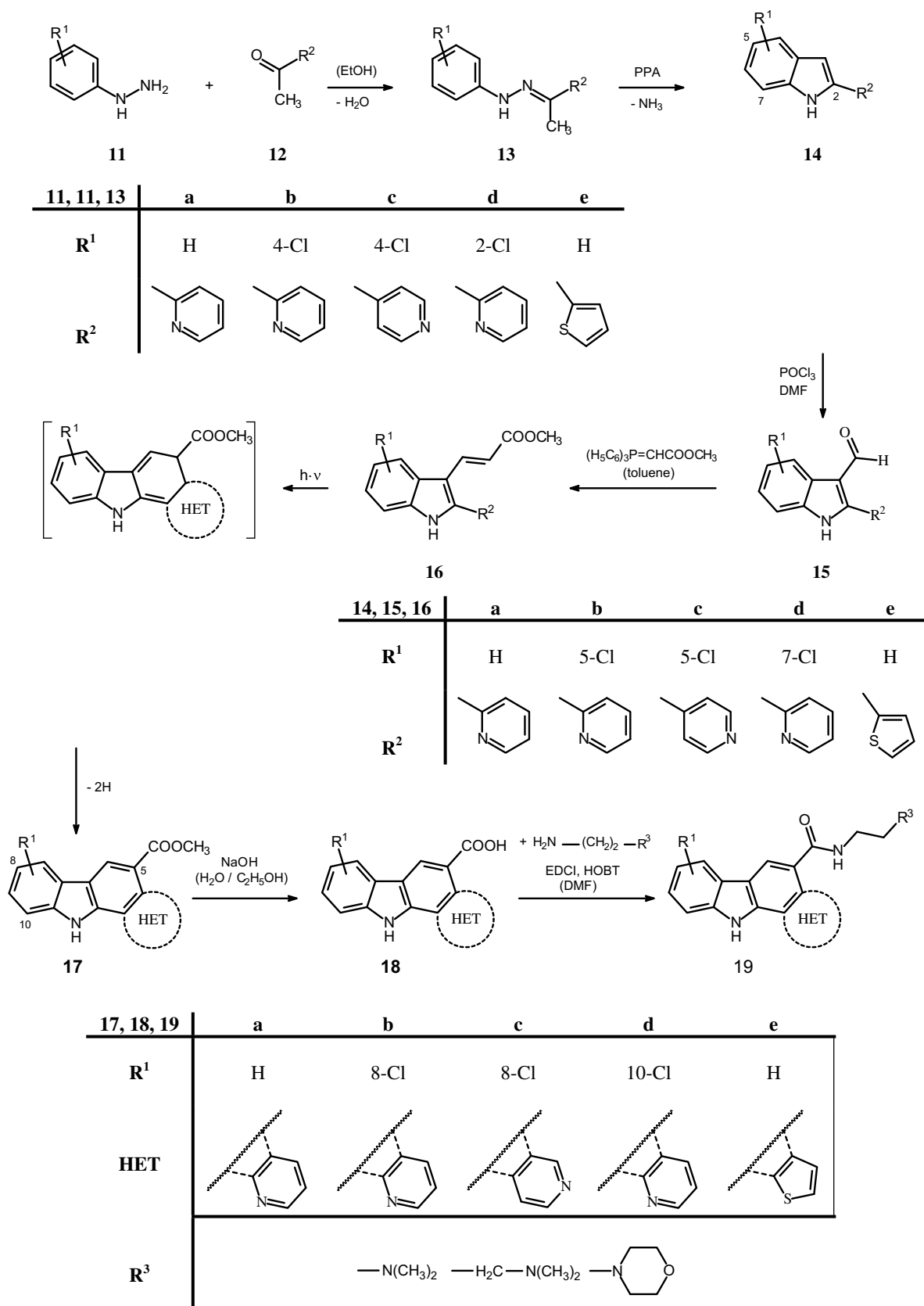
The best mean graph midpoint value MG_{MID} (activity is defined as a $\log_{10} GI_{50}$ of $< 100\text{ }\mu\text{M}$), which displays an averaged activity parameter over all cell lines, is -5.6 for the chloro-substituted compound **22**. The unsubstituted pyridocarbazoles display values of -5.2 for **20** and -4.9 for **21** (Table 2). From these results, it can be concluded that a C-2 side chain gives preference to the C-3 and furthermore the chloro-derivative is more active probably as a consequence of its higher lipophilicity.

It should be mentioned that compound **20** shows high potency against an ovarian (OVCAR-3; GI_{50} [M]: 2.54×10^{-8} , $\log_{10} GI_{50}$: -7.60) and a renal (CAKI-1; GI_{50} [M]: 5.15×10^{-7} , $\log_{10} GI_{50}$: -6.28) cell line suggesting that some antitumor-type cell selectivities can be adjudged to this compound.

In order to compare the whole series, the cytotoxic effect was measured on HT-29 cell line treated with increasing concentrations of the various compounds. The corresponding GI_{50} are presented in Table 3 and evidenced that compounds **24**, **25** (and to a lesser extend compounds **22**, and **27**) are the most cytotoxic one with GI_{50} values in the micromolar range. All four compounds are chlorine-substituted molecules. Particularly, the pyrido-[4,3*a*]carbazoles **24** and **25** are more cytotoxic than their respective pyrido[2,3*a*]carbazole derivatives **22** and **23**. Surprisingly, in the dimethylamino-propyl series, the 10-chloro-substituted compound **27** is more cytotoxic ($GI_{50} = 4.5\text{ }\mu\text{M}$) than its 8-chloro-substituted derivative **23** ($GI_{50} = 9.2\text{ }\mu\text{M}$) whereas the opposite observation is made when the 8- or 10-chloro-substitution are present in the dimethylamino-ethyl-substituted series **26** ($GI_{50} = 14\text{ }\mu\text{M}$) and **22** ($GI_{50} = 3.2\text{ }\mu\text{M}$).

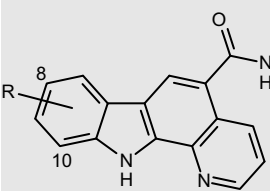
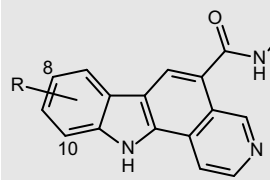
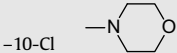
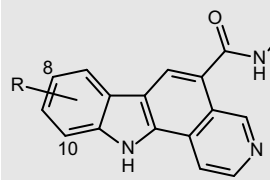
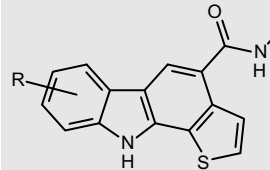
3.2. Cell cycle effect of compounds 20–29

The effect of compounds **20–29** on cell cycle was then assessed on HT-29 colon carcinoma cells. Those cells were chosen based on the interesting result obtained on cytotoxicity measurements



Scheme 3. General synthetic route to hetarene [a]-annulated carbazole amides **19** (for the formula of the final products **20–29** see Table 1).

Table 1
The final products.

	R	R'	Compound
	–H	–N(CH ₃) ₂	20
	–H	–H ₂ C–N(CH ₃) ₂	21
	–8–Cl	–N(CH ₃) ₂	22
	–8–Cl	–H ₂ C–N(CH ₃) ₂	23
	–10–Cl	–N(CH ₃) ₂	26
	–10–Cl	–H ₂ C–N(CH ₃) ₂	27
	–10–Cl		29
	–8–Cl	–N(CH ₃) ₂	24
	–8–Cl	–H ₂ C–N(CH ₃) ₂	25
	–H	–H ₂ C–N(CH ₃) ₂	28
	–H	–H ₂ C–N(CH ₃) ₂	28

(Tables 2 and 3). Results in Fig. 1 evidenced a strong accumulation of cells in G2/M phases using the unsubstituted pyridocarbazoles **20** and **21** with a very strong reduction of cells in G1 phase. By contrast, cells treated with the chloro-pyridocarbazole compounds **22** and **23** first accumulate in G2/M phase and then in G1 phase. The increase in G2/M phase also correlate with a large decrease of the G1 phase and a smaller increase in the S phase portion from 20.4 ± 1.3 to 32.6 ± 0.3 and 31.7 ± 3.4 for 25 μM of unsubstituted compounds **20** and **21**, respectively, and to 37.0 ± 1.5 and 26.1 ± 0.8 for 10 μM of chloro-substituted pyridocarbazoles **22** and **23**. At higher concentrations (25 μM), the G2/M phase arrest observed using the chloro-pyridocarbazoles **22** and **23** is reduced with cells accumulating in G1 phase whereas using the unsubstituted pyridocarbazoles **20** and **21** cells stay in a large majority in G2/M

Table 2
Some results of the 60 panel NCI antitumor screening. GI₅₀: molar concentration of compounds, which induces inhibition of cell proliferation of 50%. MG_{MID}: mean graph midpoint, activity is defined as log₁₀GI₅₀ of <100 μM .

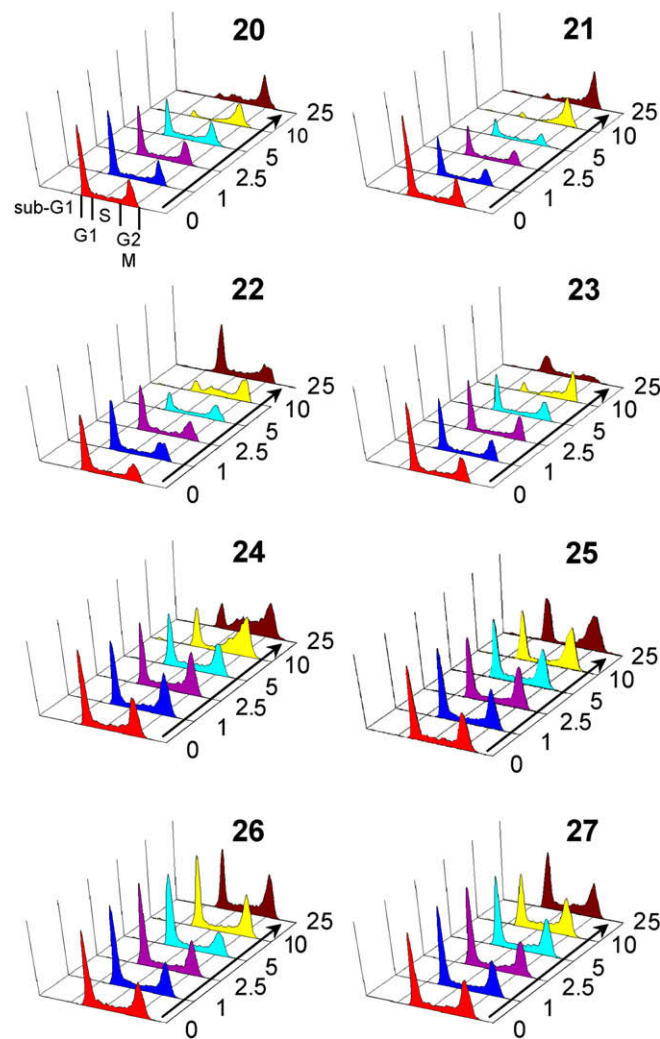
Compound	Tumor cell line	GI ₅₀ [M]	log ₁₀ GI ₅₀	MG _{MID}
20	OVCAR-3 (ovarian)	2.54×10^{-8}	–7.60	–5.2
	CAKI-1 (renal)	5.15×10^{-7}	–6.28	
	IGROV-1 (ovarian)	1.14×10^{-6}	–5.96	
	UO-31 (renal)	2.13×10^{-6}	–5.68	
	HT-29 (colon)	5.27×10^{-6}	–5.28	
21	CCRF-CEM (leukaemia)	4.31×10^{-6}	–5.37	–4.9
	COLO 205 (colon)	4.43×10^{-6}	–5.35	
	ACHN (renal)	5.24×10^{-6}	–5.28	
	HT-29 (colon)	1.03×10^{-5}	–5.99	
22	UO-31 (renal)	1.10×10^{-6}	–5.96	–5.6
	SK-MEL-5 (melanoma)	1.34×10^{-6}	–5.87	
	SW-620 (colon)	1.47×10^{-6}	–5.83	
	HT-29 (colon)	2.33×10^{-6}	–5.63	

Table 3
HT-29 cells cytotoxicity of the various compounds measured using MTS assays.

Compound	GI ₅₀ (μM)
20	11.5 ± 3.4
21	10.1 ± 1.4
22	3.20 ± 1.25
23	9.23 ± 3.12
24	1.08 ± 0.28
25	2.20 ± 1.07
26	14.0 ± 2.3
27	4.49 ± 1.48
28	10.8 ± 0.5
29	ND

phases. No differences were observed depending on the length of the side chain (compounds **20** and **22** versus **21** and **23**).

Using compound **24**, cells accumulate in G2/M phases and then in S phase. The cell cycle is less affected by treatment using compounds **25–27** with a much weaker accumulation in G2/M phase.

**Fig. 1.** Cell cycle effect of compounds **20–23** on HT-29 cells. HT-29 cells in exponential growth were exposed to the indicated concentrations of compounds **20–23** (μM) for 24 h prior to be fixed and labelled with PI for flow cytometric analysis. The various cell cycle phases and sub-G1 portion are localized in the first panel.

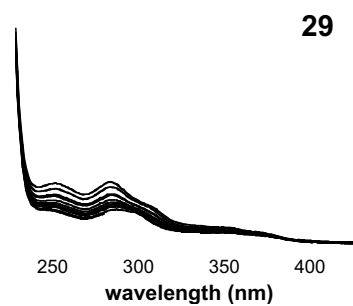
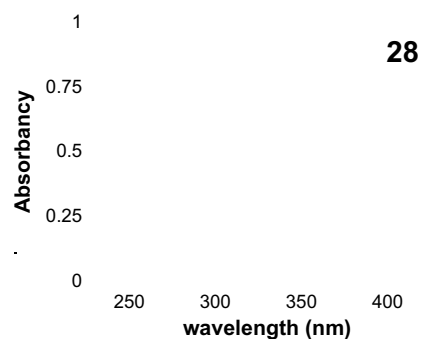
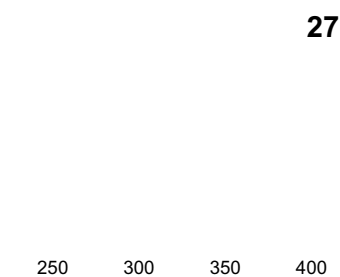
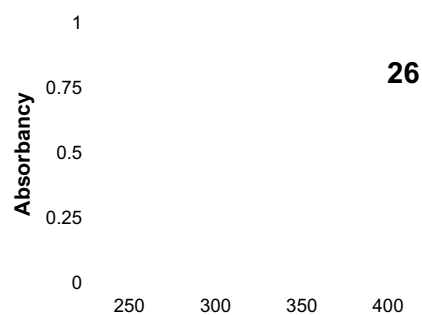
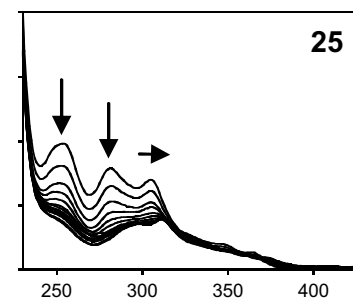
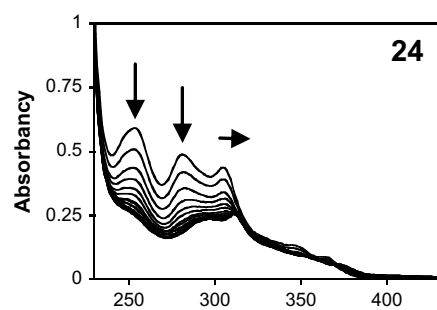
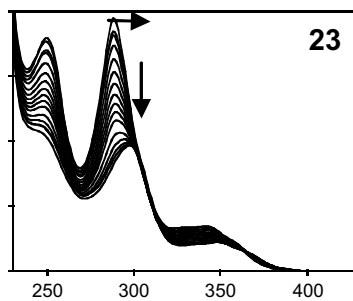
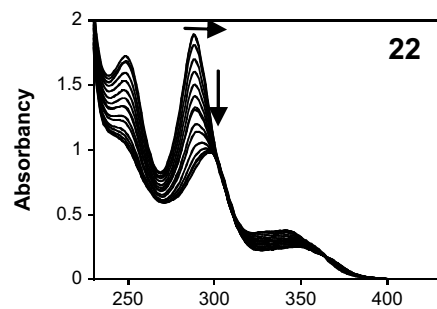
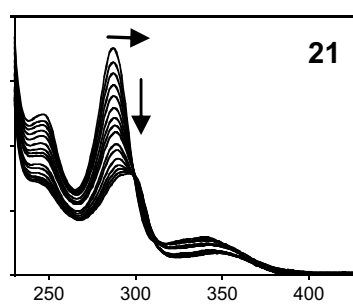
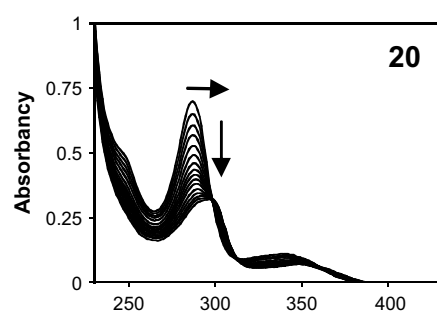


Table 4
Quantification of hypochromic and bathochromic effects.

Compound	λ_1^a (nm)	λ_2^b (nm)	$\Delta\lambda^c$ (nm)	H ^d %
20	287	293	+6	62
21	287	292	+5	56
22	288	298	+10	48
23	288	297	+9	51
24	254			56
	281			62
	305	309	+4	37
25	254			56
	281			65
	305	312	+7	25
26	286	298	+12	46
27	250			45 ^e
	286	291 ^e	+5	54 ^e
28	276	284	+8	50
29	284	297	+13	48

^a $\lambda_1 = \lambda_{\max}$ compound alone.^b $\lambda_2 = \lambda_{\max}$ compound+CT-DNA.^c $\Delta\lambda = \lambda_1' - \lambda_2$. Positive values evidenced bathochromic effects.^d Hypochromic effect $H = [100 \times (\text{Abs}_{\text{compound alone}} - \text{Abs}_{\text{compound+CT-DNA}}) / \text{Abs}_{\text{compound alone}}]$ at the specified wavelength (λ).^e Hypochromic and bathochromic effects are measured at the minimal point regarding the following increase in the γ value due to complex binding mode.

Quantification of cells in each cell cycle steps was performed as untreated cells (0) or cells treated with the increasing concentration of each compounds (arrow), as specified on the left of each graph (μM), is performed as described in the Material and methods section. The localisation of subG1, G1/G0, S, G2/M phases is specified on the first graph.

3.3. DNA binding and inhibition of topoisomerases I and II

3.3.1. UV/vis spectral absorbance

In order to address the DNA-binding ability of this series of pyridocarbazoles in the primary screening, we first looked at the modification of the absorption spectra of the various compounds in the absence and presence of increasing concentrations of calf-thymus DNA (phosphate/drug ratio from 1 to 20) based on the principle that the UV/Vis-spectra of a substance changes if it interacts with the DNA. The spectra of pyridocarbazole derivatives are presented in Fig. 2. All these compounds show hypochromic and bathochromic effects (arrows \downarrow and \rightarrow , respectively) that are quantified in Table 4. Comparison between compounds **20** and **21** to their corresponding chloro-containing derivatives **22** and **23** reveals similar hypochromic effects but different bathochromic shifts (Fig. 2 and Table 4). This bathochromic effect implies a stronger interaction between DNA and the chromophore using the chloro-substituted compounds from comparison with the unsubstituted pyridocarbazoles.

3.3.2. DNA-melting temperature

The DNA ligand affinity can be determined by UV measurement of the DNA-melting temperature, which is enhanced in case of ligand binding (base-pair separation). In order to confirm the DNA-binding ability of those compounds, we then looked at the stabilization of the DNA helix by the various hetarene annelated carbazoles using melting temperature studies. UV spectroscopic determination of the melting curve of DNA compared with the melting curve of a DNA ligand complex gives a basic information about the binding potency of a ligand to DNA [22] and is used to compare the relative affinity of a series of derivatives. The ΔT_m values ($T_m[\text{CT-DNA+drug}] - T_m[\text{CT-DNA alone}]$) were determined using calf-thymus DNA (CT-DNA) and poly(dAdT)₂ at DNA/drug ratio from 0.1 to 1. A ΔT_m value of more than 10 is a convenient sign for

a good DNA binding of the ligand. Table 5 represents the ΔT_m data of this series of the new compounds.

Derived from these data, all compounds but compound **29** reflect a significant affinity to the poly(dAdT)₂-DNA sequence (ΔT_m values $> 18^\circ\text{C}$). Comparison between ΔT_m values obtained from unsubstituted (**20**, **21**) and chloro-substituted pyridocarbazoles (**22**, **23**) clearly reveals the increase of DNA binding caused by the halogen atom. Both ΔT_m values of poly(dAdT)₂ and CT-DNA confirm this structure-activity relationship. It is mentioned that the chloro derivatives possess a higher DNA-binding affinity as the leading substance ellipticine (**1**), probably caused by their polar hydrophobicity. Concerning the length of the amidic chain, no obvious preference could be noticed from comparison of the relative affinity for DNA of compounds **20**, **22** and **24** versus **21**, **23** and **25**, respectively. However, comparison of the relative affinity for CT-DNA or poly(dAdT)₂ of compounds **26** and **27** evidenced an increase in the DNA affinity in the presence of a dimethylamino-propyl chain (**27**) instead of a dimethylamino-ethyl one (**26**). For this latter, the reduced DNA affinity could also be attributed to the orientation of the chlorine on the carbazole ring. Indeed, comparison of the relative DNA affinity for compounds **22** and **26** enlightens a decrease in DNA-binding potency when the chlorine is substituted at position 10 (**26**) instead of position 8 (**22**). The integration of a π -electron rich thiophene moiety (**28**) does not enhance the affinity for DNA compared to its pyrido analogues. Evidently, the electron density of the chromophoric system is not as determining for the DNA interaction as the introduction of a more lipophilic group. Finally, the presence of dimethyl-amine at the end of the lateral chain is, as attempted, crucial for the DNA binding as evidenced from comparison of the results using compounds **26** and **29**, in correlation with previous observation using compounds **8** and **9** lacking any side chain and that failed to induce any ΔT_m values.

3.4. Fluorescence studies

Compounds **20–25** and **28** present intrinsic fluorescence properties which could be used to evaluate their respective DNA-binding propensities (Fig. 3). Compounds chloro substituted in position 10 are not fluorescent. From the titration of compounds **24** and **25**, the emission maxima undergoes a clear red shift after binding to increasing concentration of CT-DNA, reflecting a more polar environments. The additional decrease of the fluorescence intensities indicates a marked quenching upon binding to the DNA. The quenching constant K_{sv} was deduced from Stern–Volmer plots to be 6.72×10^3 and $9.95 \times 10^3 \text{ M}^{-1}$ for compounds **24** and **25**,

Table 5

Variation of DNA-melting temperature ΔT_m [$^\circ\text{C}$] of calf-thymus DNA and poly(dAdT)₂ from complexation with various pyridocarbazoles (**20–27**, **29**) and a thienocarbazole (**28**). r = molar ratio of ligand/DNA.

Compound	ΔT_m ($^\circ\text{C}$)							
	CT-DN				Poly(dAdT) ₂			
	r				r			
	0.1	0.25	0.5	1	0.1	0.25	0.5	1
20	0	3.0	2.9	7.3	2.9	11.8	14.5	18.9
21	0	4.4	4.4	7.3	2.9	8.9	11.6	17.5
22	1.5	7.4	7.3	11.7	6.1	14.7	18.9	24.9
23	3.0	7.4	8.8	13.2	6.1	9.2	20.4	27.8
24	5.3	7.9	11.2	15.1	11.6	18.9	24.7	29.6
25	3.6	6.6	10.7	13.9	10.3	17.3	22.7	28.3
26	1.1	1.5	5.1	7.9	2.8	6.2	13.6	8.8
27	2.6	5.0	10.4	13.8	9.7	17.6	23.6	29.8
28	0	1.5	4.4	5.8	5.9	11.9	16.4	20.9
29	0	0.7	0.4	0.6	2.1	3.9	5.3	5.3

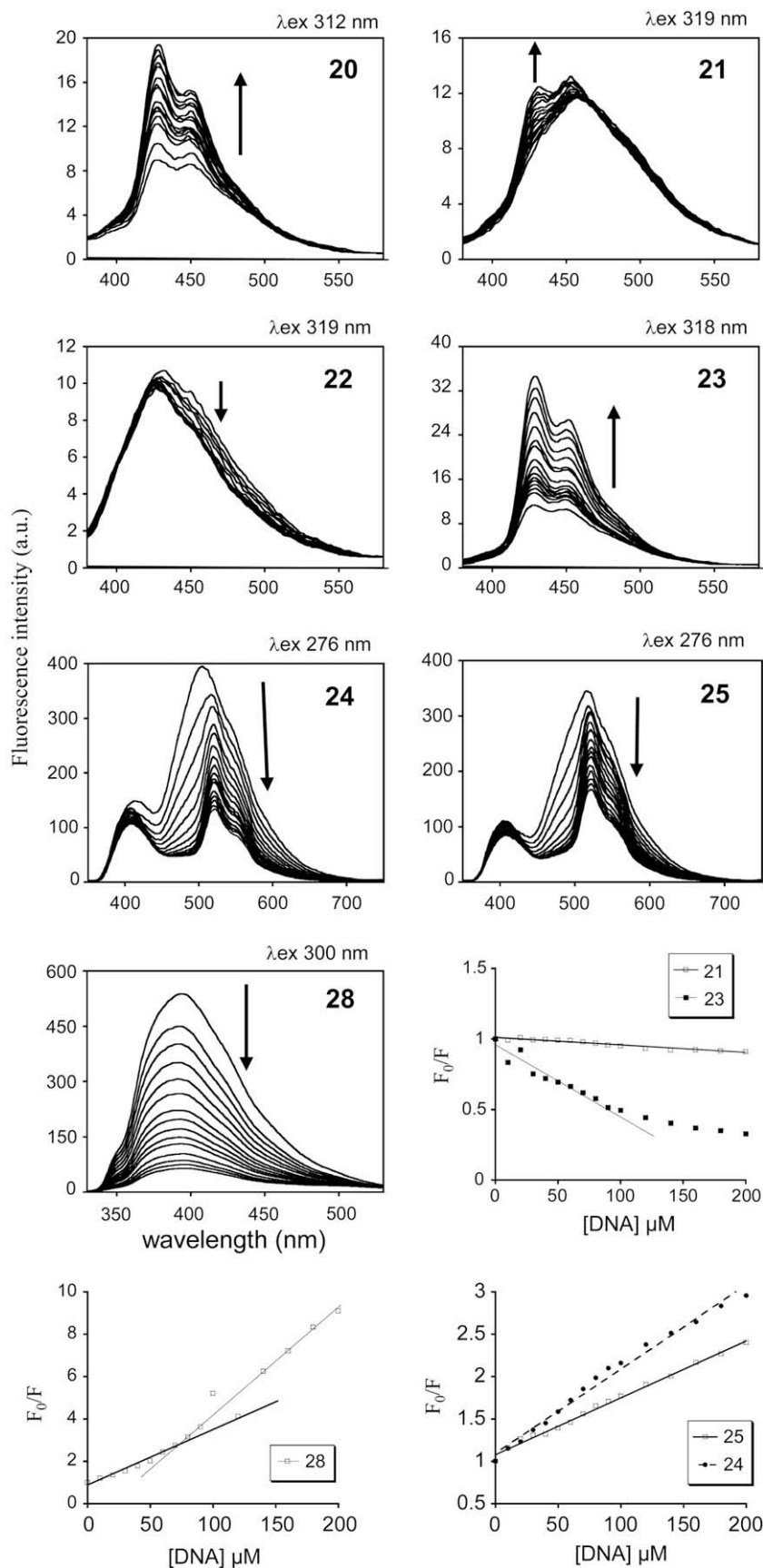


Fig. 3. Fluorescence spectra of the various pyridocarbazoles upon incubation with graded concentrations of CT-DNA. A fixed concentration of the various derivatives (20 μM) was incubated with increasing concentrations of CT-DNA from 10 to 200 μM for a phosphate/compound ratio from 0.4 to 8. Arrows indicate the orientations of the fluorescence quenching (\downarrow) or enhancement (\uparrow). The excitation wavelength peaks for the various compounds are indicated at the top of the related graphs. Stern-Volmer plots expressing F_0/F as a function of the concentration of CT-DNA is used to deduce the quenching and enhancement constants for the indicated compounds on the three bottom graphs.

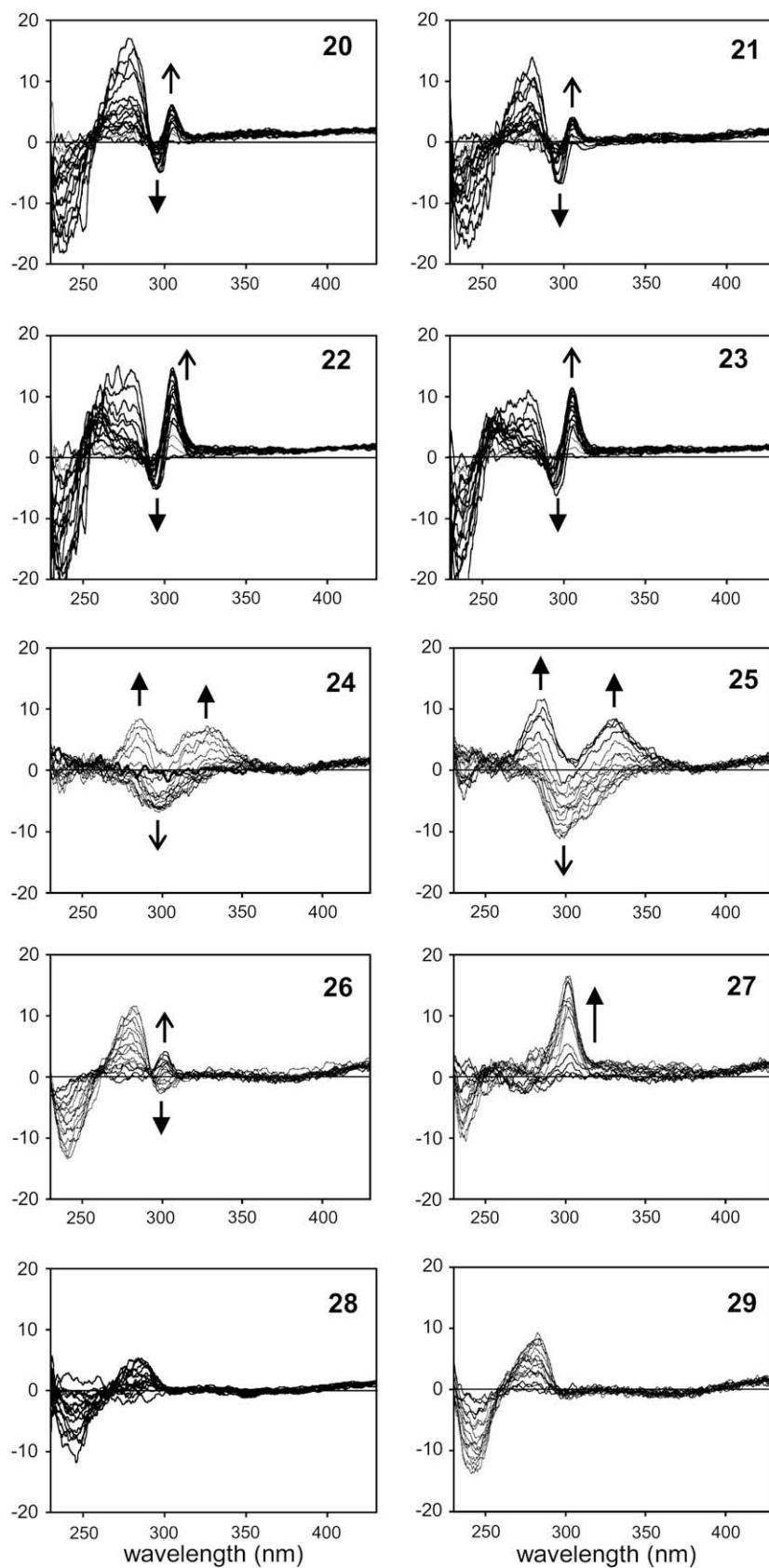


Fig. 4. Circular dichroism spectra of CT-DNA with the various pyridocarbazoles. A fixed concentration of the various derivatives (50 μM) was incubated with increasing concentrations of CT-DNA from 10 to 200 μM (phosphate/compound ratio from 0.4 to 8). Open and full arrows indicate the orientations of the induced CD at lower and upper CT-DNA concentrations, respectively.

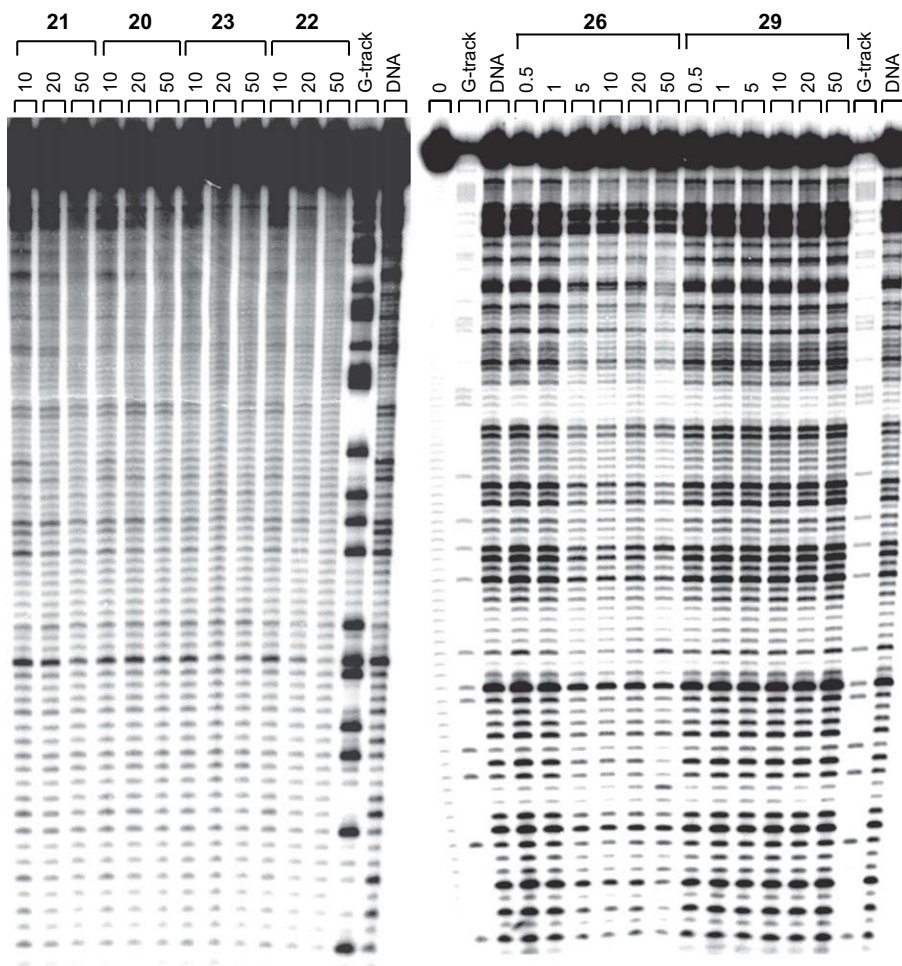


Fig. 5. Localisation of the DNA binding using DNase I footprinting analysis. The 3'-end labelled *EcoRI*-*PvuII* fragment of pBS vector was incubated with increasing amount of the drug as specified on the top of the appropriate lanes (μM) prior to be digested by DNase I. Control tracks labelled "DNA" contained no drug. Lanes labelled "G-track" were used as marker for guanine positions. Lane "0" evidenced the untreated radio-labelled DNA fragment used as quality control.

respectively. The DNA-binding mode for compound **28** appears to be more complex regarding the two slopes evidenced from Stern–Volmer plot. Such result suggests that two types of fluorophores are present in solution, one being compound **28** alone and the second being the complex formed between compound **28** and DNA base pairs. The quenching constant for compound **28** was calculated to be of $2.65 \times 10^4 \text{ M}^{-1}$ from the first points at CT-DNA concentrations up to $80 \mu\text{M}$. Contrasting with the fluorescence quenching through DNA interaction of those compounds, an enhancement of the fluorescent is observed using compounds **20** and **23**, as well as to a lesser extend using compound **21**. The enhancement constants for 8-chloro (**23**) or unsubstituted (**21**) derivatives were deduced from plotting F_0/F versus the concentration of CT-DNA to be $4.84 \times 10^{+3} \text{ M}^{-1}$ and $5.94 \times 10^{+2} \text{ M}^{-1}$, respectively.

3.4.1. Circular dichroism measurements

The binding of an achiral ligand to the chiral DNA causes an induced optical activity of the ligand. These measurements with CT-DNA were used to get an insight in the DNA-binding mode – intercalation and/or groove binding – of the various annelated carbazoles. The most common feature (compounds **20–23**) is a positive induced CD signal in the absorption area of the pyridocarbazole ligand around $\lambda = 310\text{--}315 \text{ nm}$ (Fig. 4) suggesting a groove binding of the compounds. This positive induced CD (ICD) occurs using the lowest CT-DNA concentrations and shifted to

a negative absorbance between $\lambda = 295\text{--}315 \text{ nm}$ (Fig. 4) for higher CT-DNA concentrations, suggesting the displacement of those compounds from DNA groove binding to an intercalation binding mode by increasing the concentration of base pairs (Fig. 2). Surprisingly, the pyrido-[4,3a]carbazoles **24** and **25** present different ICDs with a negative ICD at wavelength around 300 nm using the lowest CT-DNA concentrations shifting to a positive ICD at wavelength around 285 and 330 nm using the highest phosphate/drug ratio. A unique high positive ICD at 300 nm is observed using the 10-chloro-derivative **27** with a saturation of the effect for a phosphate/drug ratio of more than 4.8. The other 10-chloro-derivative **26** bearing a dimethyl-amino-ethyl arm instead of a dimethyl-amino-propyl (**27**) presents a positive ICD at the same wavelength for up to a phosphate/drug ratio of 1.2 followed by a negative ICD for higher CT-DNA/compound ratio. The morpholino derivative **29** which can be considered as a cyclic analogue of dimethylamino end of compound **26** to give abolished the formation of ICD at the wavelength of the compound, in agreement with the crucial role of the positively charged amino-termini for DNA-binding stabilization.

3.4.2. Localisation of DNA-binding site

The DNA minor groove is a good docking site for sequence selective DNA ligand. The sequence selectivity for a compound can be achieved using DNase I footprinting on a radio-labelled DNA

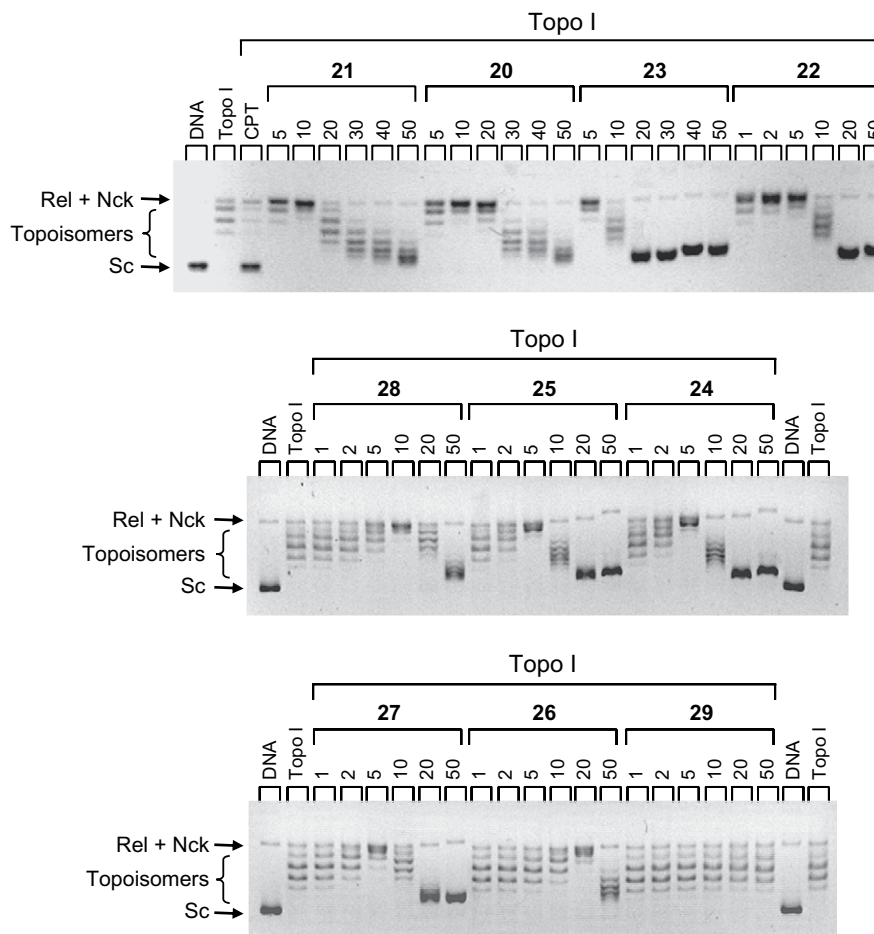


Fig. 6. Topoisomerase I-induced DNA relaxation. The effect of the various pyridocarbazoles and the thienocarbazoles on the relaxation of supercoiled plasmid DNA by topoisomerase I was established using native supercoiled pUC19 DNA (130 ng; lanes DNA) incubated with topoisomerase I in the absence (lanes Topo I) or presence of increasing concentrations (μM) of the various compounds. The different forms of plasmid DNA were separated by electrophoresis on a 1% agarose gel which was then stained with ethidium bromide. Rel, relaxed; Sc, supercoiled; Nck, nicked.

fragment. We evaluated the potential for sequence selective binding of this series of compounds on a 117 bp 3'-end labelled DNA fragment (Fig. 5). Incubation of increasing concentrations of each compounds failed to evidence any sequence selectivity but none-specific DNA interaction as attempted for DNA-intercalating compounds. The non-specific DNA binding can particularly well be seen using compounds **20–27** whereas compound **28** only weakly affect the DNase I activity and compound **29** totally failed to modify the DNA cleavage profile. Those results are in perfect correlation with previous observation from spectroscopic analysis.

The 3'-end labelled *EcoRI*-*PvuII* fragment of pBS vector was incubated with increasing amount of the drug as specified on the top of the appropriate lanes (μM) prior to be digested by DNase I. Control track labelled "DNA" contained no drug. Lanes labelled "G-track" were used as marker for guanine positions. Lane "0" evidenced the untreated radio-labelled DNA fragment used as quality control.

3.4.3. Inhibition of topoisomerases I and II

In order to get a further insight in the mode of binding of the pyridocarbazole derivative on DNA, we used the DNA relaxation properties of topoisomerase I. This method is a powerful approach to evidence DNA-intercalation process as an enhancer of DNA relaxation creating more relaxed topoisomers from topoisomerase

I-mediated cleavage of supercoiled DNA. As presented in Fig. 6, all compounds but compound **29** present a change in the topoisomer profile from negatively supercoiled to relaxed DNA (Rel) and back to (positively) supercoiled position (Sc). Those DNA relaxation profiles suggest that the compounds are potent DNA base pair intercalators thus acting on the twist of the DNA helix. The lack of DNA relaxation profile for compound **29** is in agreement with previous results evidencing no DNA double strand stabilization (Table 5), which is usually strong for DNA intercalators, and no ICD in Fig. 4. Therefore, since no groove binding could be evidenced in CD measurements, the hypochromic effect seen in UV/vis absorbance measurements with compound **29** in the presence of CT-DNA could presumably only be attributed to electrostatic binding of compound **29** to the phosphate backbone. From the DNA relaxation experiment, the intercalation efficiencies could be classified from weaker to stronger: **26** < **20** < **21**, **27**, **28** < **22**, **23**, **24**, **25** and correlate with their efficiency to stabilize the DNA helix (CT-DNA and poly(dAdT)₂) evidenced using melting temperature studies: **26** < **20**, **21** < **27**, **28**, **22–25**.

Regarding the differences for DNA binding and DNA-intercalation potencies of the unsubstituted compounds **20** and **21** versus the chloro-substituted equivalent **22** and **23**, those four compounds were evaluated for topoisomerases I and II poisoning effect. From comparison with the respective reference compounds

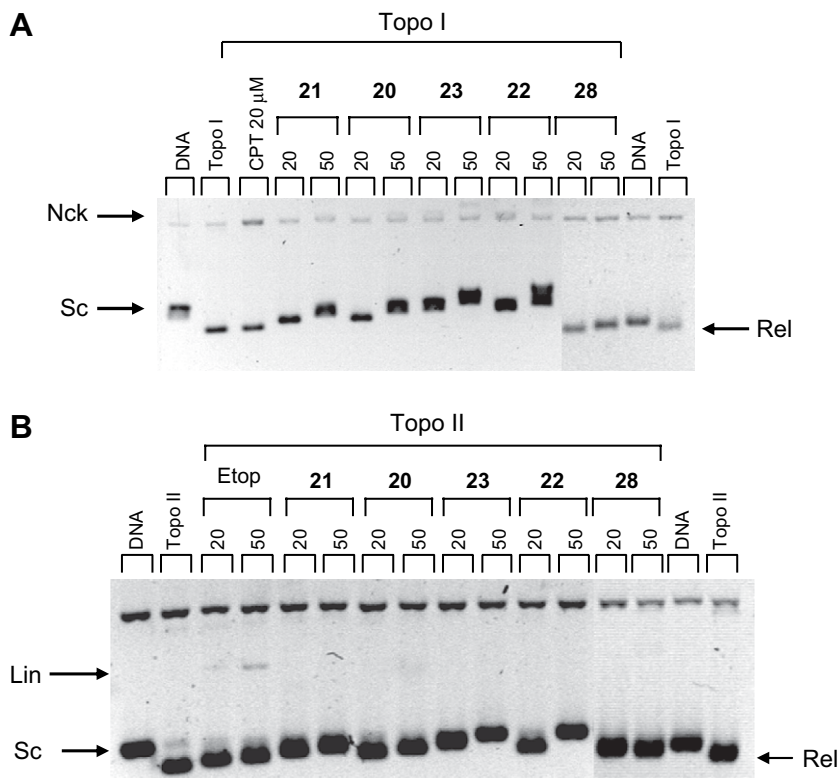


Fig. 7. Topoisomerase I (A) and II (B) poisoning effects of various pyridocarbazoles. Native supercoiled pUC19 plasmid DNA (130 ng, lanes DNA) was incubated with topoisomerase I or II in the absence (lanes Topo I or Topo II) or presence of 20 or 50 μ M of the various derivatives. Camptothecin (CPT) and etoposide (Etop) were used as specific controls. DNA samples were separated under electrophoresis on an ethidium bromide containing 1% agarose gel. The gels were photographed under UV light. Sc, supercoiled; Rel, relaxed; Nck, nicked; Lin, linear.

camptothecin (CPT, Fig. 7A) and etoposide (Etop, Fig. 7B), none of those compounds are topoisomerase I or II inhibitors as evidenced by the lack of nicking form (topoisomerase I) and double strand break form of the DNA (linear DNA, topoisomerase II). The gel shift migration of the supercoiled form correlates with the binding efficiency of the compounds: the chloro-derivatives **22** and **23** are more potent DNA-binding compounds than the unsubstituted compounds **20** and **21**, in perfect correlation with previous conclusions.

4. Discussion and conclusion

Only carbazoles **20**, **21** and the chloro derivative **22** were chosen for NCI antitumor screening. The chloro derivative **22** which displays a Mean Graph Midpoint value (MG_MID) of -5.6 proved to be the most active compound in general, whereas compound **20** shows significant activity against single ovarian (GI₅₀ [M]: 2.54×10^{-8}) and renal (GI₅₀ [M]: 5.15×10^{-7}) tumor cell lines (Table 2). Comparison of the cytotoxicity of the whole series of those newly synthesized carbazoles was established in the lab on the colon carcinoma cell line HT-29 and evidenced that compounds **22** but also compounds **24** and **25** (and to a lesser extend compound **27**) are the most cytotoxic agents in this series with GI₅₀ in the μ M range (Table 3). The cellular effects of those compounds are associated with a major G2/M phase arrest (Fig. 1).

On the basis of the UV absorption (hypochromic and bathochromic shifts) and ΔT_m values the chloro derivatives bearing a dimethylaminoalkyl-side chain reveal a significantly stronger DNA-binding potency than the basic related compounds **20** and **21**.

This could be due to an increase of the polar hydrophobicity of the chloro derivatives relatively to the unsubstituted pyridocarbazoles.

According to the DNA-melting temperature measurements, the ΔT_m values of chloro-pyridocarbazoles **22–25** and **27** range between about 25 and 30 $^{\circ}$ C, highlighting their potent DNA binding. Using this assay, the pyridocarbazoles **24** and **27** are the strongest DNA binders. Concerning the length of the amidic chain, no obvious preference could be noticed from comparison of the relative affinity for DNA of the ethylamides **20**, **22** and **24** versus the corresponding propylamides **21**, **23** and **25**, respectively. However, comparison of the relative DNA affinity for CT-DNA or poly(dAdT)₂ of compounds **26** and **27** evidenced an increased DNA affinity in the presence of a dimethylamino-propyl chain (**27**) instead of a dimethylamino-ethyl (**26**). For this latter, the reduced DNA affinity could also be attributed to the orientation of the chlorine on the carbazole ring. Indeed, comparison of the relative DNA affinity for compounds **22** and **26** enlightens a decrease in DNA-binding potency when the chlorine is substituted at position 10 (**26**) instead of position 8 (**22**). The integration of a π -electron rich thiophene moiety (**28**) does not enhance the affinity for DNA compared to its pyrido analogues. Finally, the presence of dimethyl-amine at the end of the lateral chain is, as attempted, crucial for the DNA binding as evidenced from comparison of the ΔT_m results using compounds **26** and **29**, in correlation with previous observation using compounds **8** and **9** lacking any side chain and that failed to induce any ΔT_m values.

The fluorescence titration studies are throughout positively by compounds **24**, **25** and **28** with the exception of the morpholine derivative **29**. The induced CD (ICD) on drug/DNA-binding evidences a common positive ICD signal compounds **20–23** suggesting a groove binding. By contrast, the pyrido-[4,3a]carbazoles

24 and **25** evidence negative ICD present from the lowest CT-DNA concentrations and followed by a positive ICD at the highest CT-DNA concentrations. This suggests a preliminary groove binding (amidic side chain) shifting then to an intercalation on the core of the compound between adjacent base pairs at saturating concentrations. Interestingly, the 10-chloro-derivative **27** only evidences a high positive ICD in the wavelength of the compound suggesting unique groove binding contrasting with the 10-chloro-derivative **26** presenting groove binding followed by good intercalative process. This suggests that the presence of both the chlorine and the shorter arm alters the correct positioning of the chromophore between adjacent base pairs with the chlorine protruding on one side of the DNA helix (major groove) and the dimethylaminoalkyl-side chain on the other side (minor groove), thus leading to the unique groove binding of this compound. Positioning of the chlorine at position 8 does not affect the intercalation of the chromophore within the DNA since it will be orientated properly relatively to the phosphate backbone of the DNA helix.

DNase I footprinting studies for analysing sequence selectivity of binding reveals for compounds **20–27** throughout a non-specific binding whereas carbazole **28** only weakly affects the DNase I activity and compound **29** totally failed to modify the DNA damage profile. These results are in perfect correlation with previous observations from spectroscopic analysis.

Finally, the topoisomerase I and II poisoning effects are in good correlation with other results. Indeed, the gel shift migration of the supercoiled form correlates with the binding efficiency of the compounds: the chloro derivatives **22** and **23** are more potent binding compounds than the unsubstituted compounds **20** and **21** in perfect correlation with previous conclusions.

It accomplished to synthesize a series of pyrido- and thienocarbazole amides via photochemically induced 6π -electrocyclisation. The biological and biophysical/biochemical results reveal high DNA-binding properties especially of chlorine-substituted pyridocarbazoles which exceed considerably the DNA-binding affinity of the leading substance ellipticine. The replacement of pyridine with an electron rich thiophene does not seem to bring a benefit on DNA binding. The introduction of a cyclic residue in the amidic group as side chain (morpholine) decreases DNA binding compared to acyclic series. Concerning the binding mode of active compounds **10**, we suggest groove binding and intercalation. The synthesis of regio-isomers and particularly the introduction of a further halogen atom in the chloropyridocarbazole framework give rise to develop promising candidates as potent DNA ligands.

5. Experimental

5.1. Chemistry

Melting points were measured with a Büchi 510 instrument and are uncorrected. IR spectra were recorded on a Thermoelectron Avatar 330 FT-IR using ZnSe crystal (AMTIR) (ν in cm^{-1}). ^1H NMR, ^{13}C NMR spectra including spin echo were recorded on a Bruker AC-300 apparatus (300 MHz). The samples were dissolved in CDCl_3 or $\text{DMSO}-d_6$. pd: pseudodoublet; pt: pseudotriplet. The chemical shift values are reported in parts per million (ppm, δ units) and spin-spin coupling J were listed in hertz. 70 eV EI-mass spectra were obtained with a Mascom 311-A apparatus and FD mass spectra with a Finnigan MAT 7 instrument. Photochemical apparatus: Normag company, mercury vapour medium pressure lamp with 150 W and an area of wavelength $\lambda = 200\text{--}600$ nm. Column chromatography was performed on silica gel (Merck, silica gel 60). Petrol ether of boiling point $40\text{--}60$ °C was used. Non-stoichiometric inclusion of solvent molecules gave always C, H, N analysis with divergence

$>0.3\%$. Despite using different solvent mixtures in TLC only one spot could be detected, therefore the testing compounds were considered analytically pure.

5.2. General procedure for the synthesis of hydrazones

The acetyl hetarenes [11.2 ml (100 mmol) 2- or 4-acetylpyridine resp. 10.8 ml (100 mmol) 2-acetylthiophene] were dissolved in 300 ml ethanol and the hydrazine [9.8 ml (100 mmol) phenylhydrazine resp. 17.0 g (100 mmol) 2- or 4-chlorophenylhydrazine·HCl] were added. The resulting yellow suspension was refluxed for 5 h. After cooling, the precipitated hydrazone was filtered off, washed with ethanol and petrol ether and dried.

5.2.1. 2-[(1-(2-Phenylhydrazono)ethyl)pyridine] (**13a**) [23]

Yellow solid, (19.4 g) (90 mmol) (90%), m.p. 153 °C; ^1H NMR (CDCl_3): $\delta = 2.38$ (s, 3H, CH_3), 6.89 (m, 1H, phenyl-H-4), 7.16–7.31 (m, 4H, phenyl-H), 7.71 (m, 2H, pyridyl-H), 8.14 (pd, 1H, $J = 8.1$ Hz, pyridyl-H-3), 8.56 (pd, 1H, $J = 5.0$ Hz, pyridyl-H-6).

5.2.2. 2-[1-[2-(4-Chlorophenyl)hydrazono]ethyl]pyridine (**13b**)

Yellow solid, (21.3 g) (86 mmol) (86%), m.p. 238 °C; ^1H NMR ($\text{DMSO}-d_6$): $\delta = 2.40$ (s, 3H, CH_3), 7.32 (pd, 2H, $J = 8.8$ Hz, phenyl-H-2, H-6), 7.63 (pd, 2H, $J = 8.8$ Hz, phenyl-H-3, H-5), 7.77 (pt, 1H, pyridyl-H-5), 8.24 (pd, 1H, $J = 8.1$ Hz, pyridyl-H-3), 8.43 (pt, 1H, pyridyl-H-4), 8.73 (pd, 1H, $J = 5.7$ Hz, pyridyl-H-6), 10.57 (s, NH).

5.2.3. 4-[1-[2-(4-Chlorophenyl)hydrazono]ethyl]pyridine (**13c**) [24]

Yellow solid, (21.7 g) (87 mmol) (87%), m.p. 307 °C (decomposition); ^1H NMR ($\text{DMSO}-d_6$): $\delta = 2.33$ (s, 3H, CH_3), 7.34 (pd, 2H, $J = 7.6$, phenyl-H), 7.45 (pd, 2H, $J = 7.6$, phenyl-H), 8.25 (pd, 2H, $J = 5.6$, pyridyl-H-3 + 5), 8.73 (pd, 2H, $J = 5.6$, pyridyl-H-2 + 6), 10.55 (s, NH).

5.2.4. 2-[1-[2-(2-Chlorophenyl)hydrazono]ethyl]pyridine (**13d**)

Yellow solid, (21.6 g) (88 mmol) (88%), m.p. 246 °C (decomposition); ^1H NMR ($\text{DMSO}-d_6$): $\delta = 2.44$ (s, 3H, CH_3), 6.97 (m, 1H, phenyl-H), 7.34 (m, 1H, phenyl-H), 7.43 (m, 1H, phenyl-H), 7.73 (m, 1H, phenyl-H), 7.96 (pd, 1H, $J = 8.1$ Hz, pyridyl-H), 8.30 (m, 2H, pyridyl-H), 8.72 (pd, 1H, $J = 5.5$ Hz, pyridyl-H), 8.92 (s, NH).

5.2.5. 2-[1-(2-Phenylhydrazono)ethyl]thiophene (**13e**) [25]

Yellow solid, (17.5 g) (81 mmol) (81%), m.p. 94 °C; ^1H NMR ($\text{DMSO}-d_6$): $\delta = 2.25$ (s, 3H, CH_3), 6.34 (m, 1H, thienyl-H), 7.01 (m, 1H, thienyl-H), 7.12–7.24 (m, 5H, phenyl-H), 7.39 (pd, 1H, thienyl-H-5), 8.92 (s, NH).

5.2.6. 2-Pyridin-2-yl-indole (**14a**) [26]

40 ml polyphosphoric acid was added into a beaker and heated under continuous stirring at $100\text{--}120$ °C. 4.2 g (20 mmol) 2-[1-(2-Phenylhydrazono)ethyl]pyridine (**13a**) was added in small amounts over a period of 10 min and the brown liquid was kept at m.p. 120 °C for 30 min. After cooling the mixture was hydrolyzed carefully with ice and neutralized with aqueous sodium hydroxide. The resulting yellow solid was filtered and refluxed in 300 ml acetone for about 10 min. The hot suspension was filtered and the solution was evaporated to dryness. The residue was chromatographed on silica gel (petrol ether/ethyl acetate (3:1)). White solid (2.0 g) (10.3 mmol) (52%), 152 °C; ^1H NMR (CDCl_3): $\delta = 7.05$ (m, 1H, indole-H-3), 7.11–7.26 (m, 3H, indole-H-5-7), 7.37 (pd, 1H, $J = 8.1$ Hz, indole-H-4), 7.67–7.75 (m, 2H, pyridyl-H-4 + 5), 7.83 (pd, 1H, $J = 8.1$ Hz, pyridyl-H-3), 8.59 (pd, 1H, $J = 4.3$ Hz, pyridyl-H-6), 10.23 (s, N-H); EI-MS: m/z 194 [M^+], $\text{C}_{13}\text{H}_{10}\text{N}_2$.

5.2.7. 5-Chloro-2-(pyridin-2-yl)-indole (**14b**)

See Section 5.3.1. 4.9 g (20 mmol) 2-[1-[2-(4-chlorophenyl)hydrazono]ethyl]pyridine (**13b**). The resulting yellow solid was filtered and refluxed in 200 ml ethanol instead of acetone for about 10 min. White solid (2.6 g) (11.4 mmol) (57%), m.p. 172 °C; ¹H NMR (CDCl₃): δ = 6.95 (m, 1H, indole-H-3), 7.13–7.28 (m, 3H, indole-H-4, 6, 7), 7.60 (m, 1H, pyridyl-H-3), 7.71–7.81 (m, 2H, pyridyl-H-4 + 5), 8.57 (m, 1H, pyridyl-H-6), 10.06 (s, N-H); EI-MS: *m/z* 228.1 [M⁺], C₁₃H₉ClN₂.

5.2.8. 5-Chloro-2-(pyridin-4-yl)-indole (**14c**)

See Section 5.3.1. 4.9 g (20 mmol) 4-[1-[2-(4-chlorophenyl)hydrazono]ethyl]pyridine (**13c**). The temperature was kept at m.p. 140 °C for 30–45 min. The resulting yellow solid was filtered and dissolved in 100 ml dimethyl formamide. The solution was evaporated under vacuum to dryness and chromatographed on silica gel (ethyl acetate/ethanol (2:1)). White solid (2.4 g) (10.5 mmol) (53%), 260 °C (decomposition); ¹H NMR (DMSO-*d*₆): δ = 7.14 (m, 2H, indole-H-3 + 6), 7.45 (pd, 1H, *J* = 8.6 Hz, indole-H-7), 7.63 (pd, 1H, *J* = 1.9 Hz, indole-H-4), 7.91 (pd, 2H, *J* = 6.0, pyridyl-H-3 + 5), 8.61 (pd, 2H, *J* = 6.0, pyridyl-H-2 + 6), 12.03 (s, N-H); ¹³C NMR (DMSO-*d*₆): δ = 99.9 (t), 111.2 (t), 119.6 (2 t), 120.2 (t), 123.5 (t), 124.6 (q), 129.7 (q), 136.3 (q), 136.6 (q), 137.2 (q), 150.8 (2 t); FD-MS: *m/z* 228.3 [M⁺], C₁₃H₉ClN₂.

5.2.9. 7-Chloro-2-(pyridin-2-yl)-indole (**14d**)

See Section 5.3.1. 4.4 g (20 mmol) 2-[1-[2-(4-chlorophenyl)hydrazono]ethyl]pyridine (**13d**). The reaction time of cyclization was limited to 15 min. After neutralization the crude product is extracted three times with ethyl acetate. The combined organic solutions were dried with magnesium sulfate and after removing of the solvent the residue was recrystallized with methanol. White solid (2.8 g) (12.2 mmol) (61%), m.p. 121 °C; ¹H NMR (CDCl₃): δ = 7.02–7.07 (m, 2H, indole-H-3 + 5), 7.17–7.25 (m, 2H, indole-H-4 + 6), 7.54 (pd, 1H, *J* = 7.9 Hz, pyridyl-H-3), 7.69–7.80 (m, 2H, pyridyl-H-4 + 5), 8.59 (pd, 1H, *J* = 5.0, pyridyl-H-6), 9.76 (s, N-H); FD-MS: *m/z* 199.1 [M⁺], C₁₂H₉NS.

5.2.10. 2-Thiophen-2-yl-indole (**14e**) [27]

See Section 5.3.1. 4.0 g (20 mmol) 2-[1-(2-phenylhydrazono)ethyl]thiophene (**13e**). The reaction time of cyclization was limited to 15 min. White solid (1.9 g) (9.6 mmol) (48%), m.p. 165 °C; ¹H NMR (DMSO-*d*₆): δ = 6.65 (s, 1H, indole-H-3), 6.98 (m, 1H, indole-H), 7.06–7.14 (m, 2H, indole-H), 7.35 (pd, 1H, *J* = 7.9, indole-H-7), 7.50 (m, 3H, thophene-H), 11.55 (s, N-H); FD-MS: *m/z* 228.1 [M⁺], C₁₃H₉ClN₂.

5.3. General procedure for the synthesis of 2-(pyridinyl)-1H-indole-3-carbaldehydes

1.94 g of the indole **14a** resp. 2.28 g of the chloro-indoles **14b–d** (10 mmol) were dissolved in 10 ml of dry DMF under nitrogen atmosphere and cooled down to –5 °C. 1.12 ml (12 mmol) POCl₃ were added dropwise over a period of 10 min where the temperature had to be kept under 5 °C. The suspension was stirred for 30 min at 0 °C, 30 min at room temperature and further 4 h at 90 °C. Subsequent the mixture was hydrolyzed carefully with water and neutralized with aqueous sodium hydroxide solution (20%). The suspension was filtered, the filtrate extracted with ethyl acetate and the organic phase combined with the solid. The solvent of the suspension was evaporated and the precipitate was chromatographed on silica gel.

5.3.1. 2-(Pyridin-2-yl)-indole-3-carbaldehyde (**15a**) [28]

See Section 5.4. The chromatographic isolation was performed with ethyl acetate/petrol ether (2:1). Bright yellow solid (0.9 g) (41%) (4.1 mmol), m.p. 213 °C; ¹H NMR (DMSO-*d*₆): δ = 7.22–7.33 (m, 2H, indole-5 + 6), 7.54 (m, 2H, indole-H-7, pyridyl-H-3), 8.01–8.11 (m, 2H, pyridyl-H-4 + 5), 8.24 (pd, 1H, *J* = 7.4 Hz, indole-H-4), 8.79 (pd, 1H, *J* = 4.8 Hz, pyridyl-H-6), 10.59 (s, 1H, formyl-H), 12.22 (s, 1H, N-H); EI-MS: *m/z* 222.1 [M⁺], C₁₄H₁₀N₂O.

5.3.2. 5-Chloro-2-(pyridin-2-yl)-indole-3-carbaldehyde (**15b**)

See Section 5.4. The chromatographic isolation was performed with ethyl acetate/petrol ether (2:1). Bright yellow solid (1.2 g) (47%) (4.7 mmol), m.p. 290 °C (decomposition); ¹H NMR (DMSO-*d*₆): δ = 7.32 (pd, 1H, *J* = 8.8 Hz, indole-H-6), 7.53–7.58 (m, 2H), 8.06 (pd, 1H, *J* = 1.8 Hz, pyridyl-H-4), 8.11 (m, 1H), 8.21 (pd, 1H, 1H, *J* = 1.8 Hz, pyridyl-H-3), 8.80 (pd, 1H, *J* = 4.8 Hz, pyridyl-H-6), 10.55 (s, 1H, formyl-H), 12.77 (s, 1H, N-H); FD-MS: *m/z* 256.0 [M⁺], C₁₄H₉ClN₂O.

5.3.3. 5-Chloro-2-(pyridin-4-yl)-indole-3-carbaldehyde (**15c**)

See Section 5.4. The chromatographic isolation was performed with ethyl acetate/ethanol (15:1). Bright yellow solid (1.0 g) (39%) (3.9 mmol), m.p. 275 °C (decomposition); ¹H NMR (DMSO-*d*₆): δ = 7.33 (pd, 1H, *J* = 8.8 Hz, indole-H-6), 7.55 (pd, 1H, *J* = 8.8 Hz, indole-H-7), 7.79 (pd, 2H, *J* = 5.9 Hz, pyridyl-H-3 + 5), 8.19 (pd, 1H, *J* = 1.9 Hz, indole-H-4), 8.78 (pd, 2H, *J* = 5.9 Hz, pyridyl-H-2 + 6), 10.01 (s, 1H, formyl-H), 12.10 (s, 1H, N-H); ¹³C NMR (DMSO-*d*₆): δ = 114.2 (t), 114.3 (q), 120.6 (q), 124.3 (q), 124.7 (q), 127.1 (2t), 127.7 (t), 135.0 (t), 137.0 (t), 146.6 (2t), 150.6 (q), 185.7 (q); FD-MS: *m/z* 256.7 [M⁺], C₁₄H₉ClN₂O.

5.3.4. 7-Chloro-2-(pyridin-2-yl)-indole-3-carbaldehyde (**15d**)

See Section 5.4.1. The chromatographic isolation was performed with petrol ether/ethyl acetate (1:1). Bright yellow solid (1.1 g) (43%) (4.3 mmol), 256 °C (decomposition); ¹H NMR (DMSO-*d*₆): δ = 7.22 (m, 1H, indole-H), 7.41 (m, 1H), 7.59 (m, 1H), 8.08 (m, 1H), 8.20 (m, 2H, pyridyl-H), 8.79 (m, 1H, pyridyl-H-6), 10.49 (s, 1H, N-H), 12.67 (s, 1H, formyl-H); FD-MS: *m/z* 256.1 [M⁺], C₁₄H₉ClN₂O.

5.3.5. 2-(Thiophen-2-yl)-indole-3-carbaldehyde (**15e**) [27]

2.5 ml (26.5 mmol) POCl₃ were added dropwise to 1 ml (13 mmol) DMF at 0 °C. Subsequently a solution of 2.0 g (10 mmol) **14e** in 10 ml dry diethyl ether was added slowly at 0 °C. The mixture was stirred 30 min at 0 °C and after warming up at room temperature it was heated for 3 h at 90–100 °C. The reaction was stopped by adding 30 ml ice water and neutralized with aqueous sodium hydroxide solution (20%). The suspension was extracted three times with CH₂Cl₂ and after drying of the combined organic phases. The solvent of the suspension was evaporated and the precipitate recrystallized in ethanol. Bright yellow solid (1.4 g) (62%) (6.2 mmol), m.p. 228 °C; ¹H NMR (DMSO-*d*₆): δ = 7.20–7.32 (m, 3H), 7.47 (m, 1H), 7.74 (m, 1H), 7.89 (m, 1H), 8.16 (m, 1H, indole-H-4), 10.23 (s, 1H, formyl-H), 12.44 (s, 1H, N-H); ¹³C NMR (DMSO-*d*₆): δ = 112.2 (q), 113.8 (t), 121.2 (q), 124.4 (q), 126.2 (t), 128.8 (q), 130.2 (q), 130.8 (t), 136.1 (t), 136.3 (t), 141.5 (t), 141.7 (t), 186.1 (q); FD-MS: *m/z* 227.3 [M⁺], C₁₃H₉NOS.

5.4. General procedure for the synthesis of (E)-methyl 3-(2-hetarylindol-3-yl)acrylate

10 mmol of the carbaldehyde (2.2 g of **15a**, 2.6 g of **15b–d**, 2.3 g of **15e**) and 4.3 g (13 mmol) of (methoxycarbonylmethylen)-tri-phenylphosphorane are refluxed in 300 ml dry toluene for 5–6 h. The progress of the reaction was followed by TLC (silicagel, petrol

ether/ethyl acetate (2:1)). The solvent was evaporated and the residue chromatographed on silica gel.

5.4.1. (E)-Methyl-3-[2-(pyridin-2-yl)-indol-3-yl]acrylate (**16a**) [29]

See Section 5.5. The isolation was performed with petrol ether/ethyl acetate (2:1). Bright yellow solid (2.1 g) (76%) (7.6 mmol), m.p. 158 °C; ¹H NMR (CDCl₃): δ = 3.85 (s, 3H, CH₃), 6.66 (d, 1H, ³J = 16.0 Hz, =CH), 7.27–7.34 (m, 3H), 7.46 (m, 1H), 7.82–7.88 (m, 2H), 7.96 (pd, 1H, J = 7.6, pyridyl-H), 8.27 (d, 1H, ³J = 16.0 Hz, =CH), 8.70 (m, 1H), 9.97 (s, 1H, N-H); ¹³C (DMSO-*d*₆): δ = 51.1 (p), 110.9 (q), 112.4 (t), 119.9 (t), 120.2 (t), 120.6 (t), 122.7 (t), 123.0 (t), 123.3 (t), 126.7 (q), 135.2 (q), 136.3 (q), 137.5 (2t), 149.8 (t), 150.9 (q), 166.9 (q); FT-IR (cm⁻¹): 2900–3200, 1698, 1609, 1422, 1182; FD-MS: *m/z* 278.6 [M⁺], C₁₇H₁₄N₂O₂.

5.4.2. (E)-Methyl-3-[5-chloro-2-(pyridin-2-yl)-indol-3-yl]acrylate (**16b**)

See Section 5.5. The isolation was performed with ethyl acetate/petrol ether (1:1). Bright yellow solid (2.0 g) (64%) (6.4 mmol), m.p. 182 °C; ¹H NMR (DMSO-*d*₆): δ = 3.71 (s, 3H, CH₃), 6.50 (d, 1H, ³J = 16.2 Hz, =CH), 7.29 (m, 1H, indole-H-6), 7.46–7.54 (m, 2H, indole-H + pyridyl-H), 7.83 (pd, 1H, J = 7.8, pyridyl-H-3), 7.94 (m, 1H, indole-H-4), 8.03 (m, 1H, pyridyl-H), 8.46 (d, 1H, ³J = 16.2 Hz, =CH), 8.79 (pd, 1H, J = 4.0), (pyridyl-H-6), 12.38 (s, 1H, N-H); ¹³C (DMSO-*d*₆): δ = 51.5 (p), 109.7 (q), 114.5 (t), 114.5 (t), 120.2 (t), 123.8 (t), 124.0 (t), 126.4 (q), 127.2 (q), 135.6 (q), 137.8 (t), 139.0 (2t), 140.9 (q), 149.9 (q), 150.3 (t), 167.9 (q); EI-MS: *m/z* 312.1 [M⁺], C₁₇H₁₃ClN₂O₂.

5.4.3. (E)-Methyl-3-[5-chloro-2-(pyridin-4-yl)-indol-3-yl]acrylate (**16c**)

See Section 5.5. The isolation was performed with ethyl acetate/ethanol (6:1). Bright yellow solid (2.2 g) (70%) (7.0 mmol), m.p. 251 °C (decomposition); ¹H NMR (DMSO-*d*₆): δ = 4.0 (s, 3H, CH₃), 6.52 (d, 1H, ³J = 16.0 Hz, =CH), 7.31 (m, 1H, indole-H-6), 7.52 (m, 1H, indole-H-7), 7.59 (pd, 2H, J = 6.0, pyridyl-H-3 + 5), 7.77 (d, 1H, ³J = 16.0 Hz, =CH), 8.0 (m, 1H, indole-H-4), 8.79 (pd, 2H, J = 6.0, pyridyl-H-2 + 6), 12.31 (s, 1H, N-H); ¹³C (DMSO-*d*₆): δ = 51.6 (p), 109.5 (q), 114.3 (t), 144.8 (t), 120.2 (t), 122.3 (t), 123.9 (2t), 124.1 (t), 126.6 (q), 126.9 (q), 135.8 (q), 138.2 (q), 140.9 (q), 150.6 (2t), 167.7 (q); FT-IR (cm⁻¹): 2746–3120, 1704, 1622, 1597, 1299, 1283, 998, 826; FD-MS: *m/z* 312.3 [M⁺], C₁₇H₁₃ClN₂O₂.

5.4.4. (E)-Methyl-3-[7-chloro-2-(pyridin-2-yl)-indol-3-yl]acrylate (**16d**)

See Section 5.5. The isolation was performed with petrol ether/ethyl acetate (2:1). Bright yellow solid (2.1 g) (67%) (6.7 mmol), m.p. 152–155 °C; ¹H NMR (CDCl₃): δ = 3.84 (s, 3H, CH₃), 6.63 (d, 1H, ³J = 16.0 Hz, =CH), 7.17 (m, 1H, indole-H), 7.27 (m, 1H), 7.34 (m, 1H), 7.83 (m, 3H), 8.23 (d, 1H, ³J = 16.0 Hz, =CH), 8.71 (pd, 1H, J = 4.5, pyridyl-H-6), 9.91 (s, 1H, N-H); ¹³C NMR (CDCl₃): δ = 51.7 (p), 112.0 (2q), 117.5 (q), 117.7 (t), 119.6 (t), 122.4 (t), 123.4 (t), 123.7 (t), 124.0 (t), 128.3 (q), 133.7 (q), 137.3 (t), 37.7 (t), 148.5 (q), 149.4 (t), 168.2 (q); FTIR (cm⁻¹): 3391, 1710, 1615, 1429, 1292, 1163; FD-MS: *m/z* 312.4 [M⁺], C₁₇H₁₃ClN₂O₂.

5.4.5. (E)-Methyl 3-[2-(thiophen-2-yl)-indol-3-yl]acrylate (**16e**) [29]

See Section 5.5. The isolation was performed with chloroform/ethyl acetate (4:1). Bright yellow solid (1.3 g) (46%) (4.6 mmol), m.p. 172 °C; ¹H NMR (CDCl₃): δ = 3.82 (s, 3H, CH₃), 6.61 (d, 1H, ³J = 16.0 Hz, =CH), 7.18 (m, 1H), 7.26–7.34 (m, 3H), 7.41 (m, 1H), 7.48 (m, 1H), 7.95 (m, 1H), 8.15 (d, 1H, ³J = 16.0 Hz, =CH), 8.47 (s, 1H, N-H); FD-MS: *m/z* 283.5 [M⁺], C₁₆H₁₃NO₂S.

5.5. General procedure for the synthesis of hetarene annelated [a]-carbazoles via photochemical electrocycloisolation

2 mmol of the methyl-3-(2-hetaryl-indol-3-yl)acrylate **16** and some crystals of iodine were dissolved in 450 ml of the specified solvent and irradiated with a wavelength band λ = 200–600 nm at 17–20 °C. The reaction progress was controlled by TLC. After complete conversion the solvent was let off and evaporated to dryness. The resulting residue was purified by column chromatography on silica gel.

5.5.1. Methyl-11H-pyrido[2,3-a]carbazole-5-carboxylate (**17a**)

557 mg of **16a** was dissolved in 450 ml CH₂Cl₂ and irradiated for 6 h. The progress of reaction via TLC and the isolation of the pyridocarbazole by column chromatography on silica gel were performed with petrol ether/ethyl acetate (3:1). White solid (400 mg) (72%) (1.4 mmol), m.p. 228 °C; ¹H NMR (DMSO-*d*₆): δ = 3.97 (s, 3H, CH₃), 7.32 (m, 1H, H-8), 7.50 (m, 1H, H-9), 7.72 (m, 2H, H-4 + 10), 8.34 (m, 1H, H-7), 9.01 (m, 1H, H-3), 9.13 (m, 1H, H-6), 9.47 (m, 1H, H-2), 11.96 (s, 1H, N-H); ¹³C NMR (DMSO-*d*₆): δ = 52.3, 112.7, 116.3, 118.7, 120.8 (2), 122.4, 123.5, 125.4, 126.3, 126.4, 134.8, 137.1, 138.7, 139.9, 149.1, 167.4; FTIR (cm⁻¹): 3180, 2946, 1708, 1518, 1429, 1346, 1235, 1220, 1131, 1059, 727; FD-MS: *m/z* 276.6 [M⁺], C₁₇H₁₂N₂O₂.

5.5.2. Methyl-8-chloro-11H-pyrido[2,3-a]carbazole-5-carboxylate (**17b**)

625 mg of **16b** was dissolved in 450 ml CH₂Cl₂ and irradiated for 6 h. The progress of the reaction via TLC and the isolation of the chloropyridocarbazole by column chromatography on silica gel were performed with petrol ether/ethyl acetate (2:1). White solid (410 mg) (66%) (1.3 mmol), m.p. 256 °C; ¹H NMR (CDCl₃): δ = 4.06 (s, 3H, CH₃), 7.45–7.55 (m, 2H), 7.66 (m, 1H), 8.15 (m, 1H), 8.92 (m, 1H), 9.06 (m, 1H), 9.75 (m, 1H), 10.69 (s, 1H, N-H); ¹³C NMR (DMSO-*d*₆): δ = 52.3 (p), 114.1 (t), 116.9 (q), 118.0 (q), 120.5 (t), 122.7 (t), 124.8 (q), 125.1 (q), 125.7 (q), 126.2 (t), 126.8 (t), 134.9 (t), 137.1 (q), 138.4 (q), 139.4 (q), 149.2 (t), 167.2 (q); FD-MS: *m/z* 310.2 [M⁺], C₁₇H₁₁ClN₂O₂.

5.5.3. Methyl-8-chloro-11H-pyrido[4,3-a]carbazole-5-carboxylate (**17c**)

625 mg of **16c** was dissolved in 450 ml ethanol and irradiated for 6 h. The progress of reaction via TLC and the isolation of the chloropyridocarbazole by column chromatography on silica gel were performed with ethyl acetate/ethanol (3:1). White solid (390 mg) (64%) (1.3 mmol), m.p. 285–290 °C (decomposition); ¹H NMR (DMSO-*d*₆): δ = 4.00 (s, 3H, CH₃), 7.54 (m, 1H, H-9), 7.74 (m, 1H, H-10), 8.44 (m, 1H, H-1), 8.54 (m, 1H, H-7), 8.75 (m, 1H, H-2), 9.18 (m, 1H, H-6), 10.30 (m, 1H, H-4), 11.76 (s, 1H, N-H); ¹³C NMR (DMSO-*d*₆): δ = 52.5 (p), 114.0 (t), 115.6 (t), 117.8 (q), 118.2 (q), 120.8 (t), 124.5 (q), 124.7 (q), 125.5 (q), 126.6 (t), 127.4 (t), 137.3 (q), 138.4 (q), 143.4 (t), 143.5 (q), 150.5 (t), 167.2 (q); FD-MS: *m/z* 310.8 [M⁺], C₁₇H₁₁ClN₂O₂.

5.5.4. Methyl-10-chloro-11H-pyrido[2,3-a]carbazole-5-carboxylate (**17d**)

625 mg of **16d** was dissolved in 450 ml CH₂Cl₂ and irradiated for 6 h. The progress of reaction via TLC and the isolation of the chloropyridocarbazole by column chromatography on silica gel were performed with petrol ether/ethyl acetate (2:1). White solid (425 mg) (68%) (1.4 mmol), m.p. 180 °C; ¹H NMR (CDCl₃): δ = 4.06 (s, 3H, CH₃), 7.25 (m, 1H), 7.32 (m, 1H), 7.53 (m, 1H), 7.68 (m, 1H), 8.07 (m, 1H), 8.94 (m, 1H), 9.06 (m, 1H, H-6), 9.74 (s, 1H); FD-MS: *m/z* 310.0 [M⁺], C₁₇H₁₁ClN₂O₂.

5.5.5. Methyl-10H-thieno[2,3-a]carbazole-4-carboxylate (**17e**)

567 mg of **16e** was dissolved in 450 ml CH_2Cl_2 and irradiated for 3 h. The progress of reaction via TLC and the isolation of the thienocarbazole by column chromatography on silica gel were performed with petrol ether/ethyl acetate (3:1). Bright yellow solid (253 mg) (47%) (0.9 mmol), m.p. 213 °C; ^1H NMR ($\text{DMSO}-d_6$): δ = 3.95 (s, 3H, CH_3), 7.27 (m, 1H), 7.45 (m, 1H), 7.58 (m, 1H, H-9), 7.94 (pd, 1H, 3J = 5.5, H-3), 8.27 (m, 1H, H-6), 8.34 (pd, 1H, 3J = 5.5, H-2), 8.89 (m, 1H, H-5), 12.39 (s, 1H); ^{13}C NMR ($\text{DMSO}-d_6$): δ = 52.1 (p), 111.9 (t), 115.8 (q), 117.7 (q), 120.5 (t), 120.7 (t), 122.3 (t), 123.5 (q), 125.8 (t), 126.1 (t), 127.9 (t), 137.4 (q), 137.9 (q), 139.9 (q), 140.1 (q), 167.2 (q); FD-MS: m/z 281.5 [M^+], $\text{C}_{16}\text{H}_{11}\text{NO}_2\text{S}$.

5.6. General procedure for the preparation of the hetarene annelated [a]-carbazole carboxylic acids via hydrolysis

2 mmol of the hetarene annelated [a]-carbazole **17** (553 mg of **17a**, 622 mg of **17b-d**, 563 mg of **17e**) was suspended in 20 ml ethanol and 1 ml of an aqueous sodium hydroxide solution and refluxed for 2 h. The mixture was cooled down at room temperature, neutralized first with concentrated hydrochloric acid and subsequent with acetic acid. After 1 h the precipitate was filtered off, dried for 24 h by remaining at the air and then under vacuum. The purity of the free carboxylic acids was sufficient, so that they could be applied for further reactions.

5.7. General procedure for the preparation of the hetarene annelated [a]-carbazole amides by use of EDI/HOBT as coupling reagents

2.6 mmol (404 mg) 1-ethyl-3-[3-(dimethylamino)propyl]carbodiimide (EDCI), 1.045 mmol (141 mg) 1-hydroxybenzotriazole (HOBT), 1.5 mmol of the amine and 1.045 mmol of the hetarene annelated [a]-carbazole carboxylic acids **18** were dissolved in 10 ml DMF and stirred for 24 h under nitrogen atmosphere. The urea was filtered off, the filtrate was evaporated to dryness and the residue was chromatographed on silica gel (methanol/ NH_3 (25%), 97:3).

5.7.1. N-[2-(Dimethylamino)ethyl]-11H-pyrido[2,3-a]carbazole-5-carboxamide (**20**)

274 mg of **18a** and 0.2 ml *N,N*-dimethylethylenediamine were added. White solid (253 mg) (73%) (0.8 mmol), m.p. 217 °C; ^1H NMR ($\text{DMSO}-d_6$): δ = 2.29 (s, 6H, $\text{N}(\text{CH}_3)_2$), 2.58 (t, 2H, $-\text{CH}_2$ next to amine-N), 3.48 (t, 2H, $-\text{CH}_2$ next to amidic-N), 7.28 (m, 1H), 7.46 (m, 1H), 7.65 (m, 2H), 8.24 (m, 1H), 8.56 (m, 2H), 8.94 (m, 1H), 8.98 (m, 1H), 12.21 (s, 1H, indole-N-H); ^{13}C NMR ($\text{DMSO}-d_6$): δ = 37.6 (s), 45.4 (p), 58.4 (s), 112.5 (t), 118.7 (q), 120.1 (t), 120.5 (t), 120.8 (t), 121.4 (t), 123.5 (q), 124.5 (q), 125.1 (q), 125.8 (t), 135.1 (t), 136.6 (q), 137.2 (q), 139.8 (q), 148.9 (t), 168.7 (q); FD-MS: m/z 332.2 [M^+], $\text{C}_{20}\text{H}_{20}\text{N}_4\text{O}$.

5.7.2. N-[2-(Dimethylamino)propyl]-11H-pyrido[2,3-a]carbazole-5-carboxamide hydrochloride (**21**)

274 mg of **18a** and 0.2 ml *N,N*-dimethylpropylenediamine were added. White solid (280 mg) (77%) (0.8 mmol). Because of unclear correlations concerning the NMR signals of aliphatic protons in the high-field the free base had to convert into her corresponding hydrochloride. Therefore the free base was dissolved in ether and after adding some drops of ethereal HCl the salt precipitated immediately. Free base: bright yellow solid m.p. 227 °C; hydrochloride: white solid, m.p. 295 °C; ^1H NMR ($\text{DMSO}-d_6$) of the free base: δ = 1.75 (m, 2H, $\text{C}-\text{CH}_2-\text{C}$), 2.16 (s, 6H, $\text{N}(\text{CH}_3)_2$), 2.33 (t, 2H, $-\text{CH}_2$ next to amine-N), 3.39 (t, 2H, next to amidic-N), 7.28 (m, 1H), 7.46 (m, 1H), 7.66 (m, 2H), 8.25 (m, 1H), 8.53 (s, 1H), 8.65 (m, 1H), 8.90 (m, 1H), 8.98 (m, 1H), 12.21 (s, 1H, N-H); FD-MS: m/z 346.1 [M^+], $\text{C}_{21}\text{H}_{22}\text{N}_4\text{O}$; ^1H NMR ($\text{DMSO}-d_6$) of the hydrochloride:

δ = 2.03 (m, 2H, $\text{C}-\text{CH}_2-\text{C}$), 2.78 (d, 6H, $\text{N}(\text{CH}_3)_2$), 3.18 (m, 2H, $-\text{CH}_2$ next to amine-N), 3.44 (m, 2H, next to amidic-N), 7.32 (m, 1H), 7.50 (m, 1H), 7.73 (m, 2H), 8.30 (m, 1H), 8.71 (m, 1H), 8.88 (m, 1H), 9.06 (m, 2H), 10.50 (s, 1H, N-H), 12.08 (s, 1H, indole-N-H); ^{13}C NMR of the hydrochloride (methanol- d_4): 26.2 (s), 38.0 (s), 43.7 (p), 56.9 (s), 113.4 (t), 121.6 (t), 122.1 (t), 122.4 (t), 123.1 (q), 123.8 (q), 123.9 (t), 125.2 (q), 126.2 (q), 128.7 (t), 132.1 (q), 132.7 (q), 141.2 (q), 142.1 (t), 145.9 (t), 171.4 (q); FD-MS: m/z 346.1 [M^+], 347.1 [27%] $\text{C}_{21}\text{H}_{23}\text{ClN}_4\text{O}$.

5.7.3. 8-Chloro-N-[2-(dimethylamino)ethyl]-11H-pyrido[2,3-a]carbazole-5-carboxamide (**22**)

310 mg of **18b** and 0.2 ml *N,N*-dimethylethylenediamine were added. White solid (288 mg) (75%) (0.8 mmol), m.p. 255 °C; ^1H NMR ($\text{DMSO}-d_6$): δ = 2.30 (s, 6H, $\text{N}(\text{CH}_3)_2$), 2.59 (t, 2H, $-\text{CH}_2$ next to amine-N), 3.49 (t, 2H, $-\text{CH}_2$ next to amidic-N), 7.46 (m, 1H), 7.66 (m, 2H), 8.36 (m, 1H), 8.56 (m, 2H), 8.91 (m, 1H), 8.99 (m, 1H), 12.04 (s, 1H, N-H); ^{13}C NMR ($\text{DMSO}-d_6$): δ = 37.6 (s), 45.4 (p), 58.4 (s), 114.0 (t), 118.0 (q), 120.1 (t), 120.9 (t), 121.8 (t), 124.5 (q), 124.6 (q), 124.8 (q), 125.6 (q), 125.7 (t), 135.1 (t), 137.2 (q), 137.4 (q), 138.2 (q), 149.2 (t), 138.5 (q); FD-MS: m/z 366.2 [M^+], 368.3 [34%] $\text{C}_{20}\text{H}_{19}\text{ClN}_4\text{O}$.

5.7.4. 8-Chloro-N-[(2-(dimethylamino)propyl)-11H-pyrido[2,3-a]carbazole-5-carboxamide] (**23**)

310 mg of **18b** and 0.2 ml *N,N*-dimethylpropylenediamine were added. White solid (290 mg) (73%) (0.8 mmol), m.p. 256 °C; ^1H NMR ($\text{DMSO}-d_6$): δ = 1.75 (m, 2H, $\text{C}-\text{CH}_2-\text{C}$), 2.17 (s, 6H, $\text{N}(\text{CH}_3)_2$), 2.34 (t, 2H, $-\text{CH}_2$ next to amine-N), 3.38 (t, 2H, $-\text{CH}_2$ next to amidic-N), 7.46 (m, 1H), 7.66 (m, 2H), 8.37 (m, 1H), 8.57 (m, 1H), 8.62 (m, 1H), 8.87 (m, 1H), 8.99 (m, 1H), 12.04 (s, 1H, indole-N-H); ^{13}C NMR ($\text{DMSO}-d_6$): δ = 27.5 (s), 38.1 (s), 45.5 (p), 57.2 (s), 114.0 (t), 118.0 (q), 120.1 (t), 120.9 (t), 121.8 (t), 124.5 (q), 124.6 (q), 124.8 (q), 125.7 (t), 125.9 (q), 135.0 (t), 137.2 (q), 137.3 (q), 138.2 (q), 149.2 (t), 168.5 (q); FD-MS: m/z 380.2 [M^+], 382.2 [34%] $\text{C}_{21}\text{H}_{21}\text{ClN}_4\text{O}$.

5.7.5. 8-Chloro-N-[2-(dimethylamino)ethyl]-11H-pyrido[4,3-a]carbazole-5-carboxamide (**24**)

310 mg of **18c** and 0.2 ml *N,N*-dimethylethylenediamine were added. White solid (260 mg) (68%) (0.7 mmol), m.p. 289 °C; ^1H NMR (methanol- d_6): δ = 2.40 (s, 6H, $\text{N}(\text{CH}_3)_2$), 2.71 (t, 2H, $-\text{CH}_2$ next to amine-N), 3.68 (t, 2H, $-\text{CH}_2$ next to amidic-N), 7.48 (m, 1H), 7.62 (m, 1H), 8.19 (m, 1H), 8.25 (m, 1H), 8.57 (m, 2H), 9.77 (m, 1H); ^{13}C NMR ($\text{DMSO}-d_6$): δ = 7.9 (s), 45.6 (p), 58.6 (s), 113.9 (t), 115.4 (t), 118.2 (2q), 120.4 (t), 121.4 (t), 124.3 (2q), 124.8 (q), 126.2 (t), 126.7 (q), 135.2 (q), 138.2 (q), 143.5 (t), 150.9 (t), 168.3 (q); FD-MS: m/z 366.6 [M^+], 368.6 [35%] $\text{C}_{20}\text{H}_{19}\text{ClN}_4\text{O}$.

5.7.6. 8-Chloro-N-[2-(dimethylamino)propyl]-11H-pyrido[4,3-a]carbazole-5-carboxamide (**25**)

310 mg of **18c** and 0.2 ml *N,N*-dimethylpropylenediamine were added. White solid (271 mg) (71%) (0.8 mmol), m.p. 283 °C; ^1H NMR ($\text{DMSO}-d_6$): δ = 1.76 (m, 2H, $\text{C}-\text{CH}_2-\text{C}$), 2.20 (s, 6H, $\text{N}(\text{CH}_3)_2$), 2.38 (t, 2H, $-\text{CH}_2$ next to amine-N), 3.42 (t, 2H, $-\text{CH}_2$ next to amidic-N), 7.51 (m, 1H), 7.72 (m, 1H), 8.39 (m, 1H), 8.42 (m, 1H), 8.59 (m, 1H), 8.69 (m, 2H), 9.70 (m, 1H), 11.98 (s, 1H, indole-N-H); ^{13}C NMR ($\text{DMSO}-d_6$): δ = 27.3 (s), 28.0 (s), 45.4 (p), 57.1 (s), 113.9 (t), 115.4 (t), 118.2 (2q), 120.3 (t), 121.5 (t), 124.3 (2q), 124.8 (q), 126.2 (t), 126.6 (q), 135.3 (q), 138.2 (q), 143.5 (t), 150.8 (t), 168.3 (q); FD-MS: m/z 381.1 [M^+], 383.1 [36%] $\text{C}_{21}\text{H}_{21}\text{ClN}_4\text{O}$.

5.7.7. 10-Chloro-N-[2-(dimethylamino)ethyl]-11H-pyrido[2,3-a]carbazole-5-carboxamide (**26**)

310 mg of **18d** and 0.2 ml *N,N*-dimethylethylenediamine were added. Bright yellow solid (215 mg) (56%) (0.6 mmol), m.p. 199 °C;

^1H NMR (methanol- d_6): δ = 2.40 (s, 6H, $\text{N}(\text{CH}_3)_2$), 2.72 (t, 2H, $-\text{CH}_2$ next to amine-N), 3.69 (t, 2H, $-\text{CH}_2$ next to amidic-N), 7.18 (m, 1H), 7.41 (m, 2H), 7.95 (m, 1H), 8.38 (m, 1H), 8.77 (m, 2H); ^{13}C NMR (DMSO- d_6): δ = 37.8 (s), 45.6 (p), 58.5 (s), 116.9 (q), 119.3 (q), 119.4 (t), 120.6 (t), 121.2 (t), 121.8 (t), 124.9 (q), 125.5 (q), 125.6 (t), 126.6 (q), 135.1 (t), 136.8 (q), 137.1 (q), 137.4 (q), 149.1 (t), 168.4 (q); FD-MS: m/z 365.8 [M^+], 367.8 [31%] $\text{C}_{20}\text{H}_{19}\text{ClN}_4\text{O}$.

5.7.8. 10-Chloro-N-[2-(dimethylamino)propyl]-11H-pyrido[2,3-a]carbazole-5-carboxamide (**27**)

310 mg of **18d** and 0.2 ml *N,N*-dimethylpropylenediamine were added. Bright yellow solid (225 mg) (59%) (0.6 mmol), m.p. 195 °C; ^1H NMR (methanol- d_6): δ = 2.0 (m, 2H, $\text{C}-\text{CH}_2-\text{C}$), 2.42 (s, 6H, $\text{N}(\text{CH}_3)_2$), 2.65 (t, 2H, $-\text{CH}_2$ next to amine-N), 3.55 (t, 2H, $-\text{CH}_2$ next to amidic-N), 7.24 (m, 1H, H-8), 7.44 (m, 1H, H-9), 7.51 (m, 1H, H-3), 8.05 (m, 1H, H-7), 8.41 (s, 1H, H-6), 8.84 (m, 2H, H-2 + 4); ^{13}C NMR (DMSO- d_6): δ = 27.3 (s), 38.0 (s), 45.4 (p), 57.1 (s), 117.0 (q), 119.3 (q), 119.4 (t), 120.6 (t), 121.2 (t), 121.8 (t), 124.9 (q), 125.5 (q), 125.6 (t), 126.6 (q), 135.1 (t), 136.8 (q), 137.1 (q), 137.5 (q), 149.1 (t), 168.4 (q); FD-MS: m/z 380.4 [M^+], 382.4 [33%]; $\text{C}_{21}\text{H}_{21}\text{ClN}_4\text{O}$.

5.7.9. N-[3-(Dimethylamino)propyl]-10H-thieno[2,3-a]carbazole-4-carboxamide hydrochloride (**28**)

286 mg of **18e** and 0.2 ml *N,N*-dimethylpropylenediamine were added. The free base **28** was dissolved in ether and precipitated with ethereal HCl to generate the hydrochloride. Bright yellow solid (156 mg) (39%) (0.4 mmol), m.p. 243 °C (decomposition); ^1H NMR (DMSO- d_6): δ = 1.99 (m, 2H, $\text{C}-\text{CH}_2-\text{C}$), 2.78 (s, 6H, $\text{N}(\text{CH}_3)_2$), 3.16 (t, 2H, $-\text{CH}_2$), 3.42 (t, 2H, $-\text{CH}_2$), 7.26 (m, 1H), 7.43 (m, 1H), 7.58 (m, 1H), 7.82 (m, 1H), 8.15 (m, 2H), 8.56 (s, 1H), 8.71 (m, 1H), 10.15 (s, 1H, indole-N-H); ^{13}C NMR (DMSO- d_6): δ = 24.8 (s), 36.7 (s), 42.5 (p), 55.0 (s), 111.9 (t), 117.4 (q), 118.0 (t), 120.1 (t), 120.3 (t), 122.4 (q), 134.4 (q), 123.6 (q), 125.7 (t), 125.8 (t), 126.4 (t), 135.8 (q), 137.2 (q), 140.0 (q), 168.8 (q); FD-MS: m/z 351.0 [M^+]; $\text{C}_{20}\text{H}_{21}\text{N}_3\text{OS}$.

5.8. Cytotoxicity and cell cycle analysis on HT-29 cell line

HT-29 colon carcinoma cells were grown in DMEM-glutaMAX medium (Gibco) supplemented with 10% fetal calf serum (FCS), penicillin (100 IU/ml) and streptomycin (100 $\mu\text{g}/\text{ml}$) in a humidified atmosphere at 37 °C under 5% CO_2 .

The cytotoxicity of the various compounds was assessed using the MTS cell proliferation assay developed by Promega (CellTiter 96® AQueous one solution cell proliferation assay). Briefly, 3×10^3 exponentially growing HT-29 cells were seeded in 96-well micro-culture plates for 24 h prior to be subjected to treatment using graded concentrations of the tested compounds from 1 nM to 100 μM in 3 different series of duplicate or triplicate points. After 72 h of incubation at 37 °C, 20 μl of the tetrazolium dye were added to each well and the samples were incubated for a further 2 h at 37 °C. Plates were analyzed on a Labsystems Multiskan MS (type 352) reader at 492 nm. The GC_{50} was determined as the concentration for which the number of cell is one half of that obtained in the non-treated control wells (6 individual points per plate) using graphical analyses using SoftMax Pro 4.7.1 software.

For flow cytometric analysis of DNA content, 3×10^5 cells in exponential growth phase were treated with graded concentrations of the test drug for 24 h as indicated in figure legends. The cells were then washed twice with phosphate buffered saline (PBS), incubated with 100 μL of trypsin (Gibco) for 5 min at 37 °C, washed again with 500 μL of culture medium to inhibit trypsin and harvested. Cells were then fixed using 70% ethanol. Finally, 500 μL of PBS containing propidium iodide (PI, FluoProbes) at 50 $\mu\text{g}/\text{ml}$ and RNase (Sigma) at 100 $\mu\text{g}/\text{ml}$ were added for 30 min at room temperature in the darkness. Cell samples were analyzed on

a Becton Dickinson FACScan flow cytometer using the LYSYS II software. PI was excited at 488 nm and the emitted fluorescence was quantified at 620 nm on channel FL-3. WinMdi software was used to determine the percentage of cells in G1, S or G2/M phases. Each experiment was performed in duplicate.

5.9. UV/vis absorption spectroscopy and DNA-melting temperature studies

CT-DNA and double stranded poly(dAdT)₂ oligonucleotide were purchased from Sigma. CT-DNA was prepared as previously described [12]. The synthesized compounds were prepared as 10 mM solutions in DMSO and further freshly diluted in the appropriate aqueous buffer.

UV/vis spectral absorption measurement was conducted using 20 μM of the various tested drugs incubated in 1 ml of BPE buffer (6 mM Na_2HPO_4 , 2 mM NaH_2PO_4 , 1 mM EDTA, pH 7.1) in the presence or absence of increasing concentrations of CT-DNA (10, 20, 30, 40, 50, 60, 70, 80, 90, 100, 120, 140, 160, 180, 200 μM of base pairs) in a quartz cuvette of 10 mm path length. The UV/vis spectra were recorded from 230 nm to 430 nm using an Uvikon 943 spectrophotometer and are referenced against a cuvette containing DNA at the same concentration than in the sample cuvette to directly substrate intrinsic DNA absorption.

The variation of melting temperature was calculated from the melting temperature measurement of 20 μM of CT-DNA or poly(dAdT)₂ incubated alone (control T_m) or with increasing concentration of the various compounds (drug/base pair ratio of 0.1, 0.25, 0.5 or 1) in 1 ml BPE buffer. The absorbency of DNA at 260 nm was measured in quartz cells using the Uvikon 943 spectrophotometer thermostated with a Neslab RTE111 cryostat. Absorption value was measured every minute over a range of 20–100 °C with an increment of 1 °C/min. The T_m values were obtained from the midpoint of the hyperchromic transition. ΔT_m values = $T_{m[\text{Drug}+\text{DNA}]} - T_{m[\text{DNA alone}]}$.

5.10. Fluorescence spectroscopy

Fluorescence spectral measurement was recorded using 20 μM of the fluorescent drugs incubated in 1 ml of BPE buffer in the presence or absence of increasing concentrations of CT-DNA (10, 20, 30, 40, 50, 60, 70, 80, 90, 100, 120, 140, 160, 180, 200 μM of base pairs) in a quartz cuvette of 10 mm path length. The excitation wavelengths were 312 (compound **20**), 319 (compounds **21**, **22**), 318 (compound **23**), 276 (compounds **24**, **25**) and 300 nm (compound **28**). The quenching constant K_{sv} was deduced from Stern–Volmer method where the ratio of fluorescence of the compound alone (F_0) over the fluorescence of the compound in the presence of CT-DNA (F) is presented as a function of CT-DNA concentration. In this configuration, $F_0/F = 1 + K_{sv}[\text{CT-DNA}]$. The slope K_{sv} is considered as an equilibrium constant for the static quenching process.

5.11. Circular dichroism

The different drugs (50 μM) were incubated in 1 ml of sodium cacodylate (1 mM, pH 7.0) with or without (control) increasing concentration of CT-DNA (10, 20, 30, 40, 50, 60, 70, 80, 90, 100, 120, 140, 160, 180, 200 μM). The CD spectra were collected from 430 to 230 nm with a resolution of 0.1 nm, in a quartz cell of 10 mm path length, using a J-810 Jasco spectropolarimeter at 20 °C controlled by a PTC-424S/L peltier type cell changer (Jasco).

5.12. DNase I footprinting

DNase I footprinting experiments were performed essentially as described in Ref. [30]. A 117 bp DNA fragment was obtained from double digestion of the pBS plasmid (Stratagene, La Jolla, CA) at *EcoRI* and *PvuII* restriction sites for 1 h with the corresponding enzymes in their respective buffers. The generated DNA fragment was 3'-end labelled by incubation with α -[^{32}P]-dATP (3000 Ci/mmol, GE Healthcare, Buckinghamshire, England) and 10 units of Klenow enzyme (BioLabs) for 30 min at 37 °C. The 117 bp radio-labelled DNA fragment was then isomated on a 6% polyacrylamide gel under native conditions in TBE buffer (89 mM Tris base, 89 mM boric acid, 2.5 mM Na₂ EDTA, pH 8.3), cut off from the gel, crushed and dialyzed overnight against 400 μL of elution buffer (10 mM Tris-HCl pH 8.0, 1 mM EDTA, 100 mM NaCl). This suspension was separated from polyacrylamide gel by filtration through a Millipore 0.22 μm membrane. The DNA was precipitated with cold ethanol followed by centrifugation. The radio-labelled DNA fragment was then dried and the pellet dissolved in water. Appropriate concentrations of the various ligands (as indicated in the figure legends) were incubated with the 117-bp radio-labelled DNA fragment 15 min incubation at 37 °C to ensure equilibrium prior to digestion of the DNA by the addition of DNase I (final concentration 0.001 unit/ml) in 20 mM NaCl, 2 mM MgCl₂, 2 mM MnCl₂, pH 7.3. After 3 min of digestion, the reaction was stopped by freeze-drying. Samples were lyophilized and subsequently dissolved in 4 μL of denaturing loading buffer (80% formamide solution containing tracking dyes). The DNA samples were heated at 90 °C for 4 min and chilled on ice for 4 min prior to electrophoresis. DNA cleavage products were resolved under polyacrylamide electrophoresis in denaturing conditions (0.35 mm thick, 8% polyacrylamide containing 8 M urea). After a 90 min electrophoresis at 65 W in TBE buffer, gels were soaked in 10% acetic acid for 10 min, transferred to Whatman 3 MM paper and dried under vacuum at 80 °C. A Molecular Dynamics STORM 860 was used to collect data from storage screens exposed to dried gels overnight at room temperature. The identity of the bases was established from comparison of the relative position of the bands to the guanines sequencing standard (G-track) classically obtained using dimethyl-sulfate and piperidine treatment of the same DNA fragment.

5.13. Topoisomerase I-mediated DNA relaxation, topoisomerases I or II cleavage assays

Topoisomerase I-mediated DNA relaxation experiments were performed as previously described in Ref. [15] with the following modifications. Graded concentrations of the tested compounds were incubated in the presence of supercoiled pUC19 plasmid DNA (130 ng) prior to the addition of 4 units of human topoisomerase I (Topogen, USA) at 37 °C for 45 min in relaxation buffer [50 mM Tris(hydroxymethyl)aminomethane (pH 7.8), 50 mM KCl, 10 mM MgCl₂, 1 mM dithiothreitol, 1 mM EDTA and 1 mM ATP]. The reactions were stopped upon addition of SDS to 0.25% and proteinase K to 250 $\mu\text{g}/\text{mL}$ and incubation of the samples for 30 min at 50 °C. 3 μL of the electrophoresis dye mixture were added to the DNA samples which were then loaded on a 1% agarose gel. The various DNA forms were separated by electrophoresis at room temperature for 2 h at 120 V in TBE buffer (89 mM Tris-borate pH 8.3, 1 mM EDTA). Gels

were run without ethidium bromide and then stained using a bath containing ethidium bromide. For topoisomerase I DNA cleavage assays, the samples were treated as for the relaxation assays but loaded on a 1% agarose gel that was prepared with ethidium bromide. Camptothecin (CPT, 20 μM) was used as a control for topoisomerase I poisoning effect. For topoisomerase II DNA cleavage assays, supercoiled pUC19 plasmid (130 ng) was incubated with 20 or 50 μM of compounds **20–24**, or etoposide as a control, prior to the addition of 4 units of human topoisomerase II (Topogen, USA) at 37 °C for 45 min in the appropriate cleavage buffer. SDS (0.25%) and proteinase K (250 $\mu\text{g}/\text{mL}$) were then added to stop the reaction during 30 min at 50 °C. DNA samples were loaded on 1% agarose gels containing ethidium bromide for 2 h at 120 °C in TBE buffer. After migration, both gels were washed and photographed under UV light.

Acknowledgments

This work was supported by grants from the Ligue Nationale contre le Cancer (Comité du Nord) and the IRCL to M.-H.D.-C. G.L. thanks the Université de Lille 2 and the Conseil Régional Nord/Pas-de-Calais for a Ph.D. fellowship.

References

- [1] H. Mastalarz, R. Jasztold-Howorko, F. Rulko, A. Croisy, D. Carrez, Arch. Pharm. Pharm. Med. Chem. 337 (2004) 434–439.
- [2] M.M. Harding, A.R. Grummitt, Mini Rev. Med. Chem. 3 (2003) 67–76.
- [3] A. Pierré, G. Atassi, M. Devissaguet, E. Bissagli, Drugs Future 22 (1997) 53–59.
- [4] G.W. Gribble, The Alkaloids, In: Synthesis and Antitumor Activity of the Ellipticine Alkaloids and Related Compounds, vol. 39 (1990).
- [5] J. Rouessé, M. Spielman, F. Turpin, T. Le Chevalier, M. Azab, J.M. Mondésir, Eur. J. Cancer 29A (1993) 856–859.
- [6] U. Pindur, Pharm. Unserer Zeit. 16 (1987) 47–52.
- [7] M.F. Brana, M. Cacho, A. Gradillas, B. de Pascual-Teresa, A. Ramos, Curr. Pharm. Des. 7 (2001) 1745–1780.
- [8] C. Guillonneau, A. Nault, E. Raimbaud, S. Léonce, L. Kraus-Berthier, A. Pierré, S. Goldstein, Bioorg. Med. Chem. 13 (2005) 175–184.
- [9] R. Jasztold-Howorko, C. Landras, A. Pierré, G. Atassi, N. Guilbaud, L. Kraus-Berthier, S. Léonce, Y. Rolland, J.F. Prost, E. Bisagni, J. Med. Chem. 37 (1994) 2445–2452.
- [10] C. Asche, M. Demeunynck, Anti-cancer agents, Med. Chem. 7 (2007) 247–267.
- [11] D. Pelaprat, R. Oberlin, I. Le Guen, B.P. Roques, J.B. Pecq, J. Med. Chem. 23 (1980) 1330–1335.
- [12] U. Pindur, T. Lemster, Recent Res. Dev. Org. Bioorg. Chem. 1 (1997) 33–53.
- [13] T. Lemster, U. Pindur, Recent Res. Dev. Org. Bioorg. Chem. 5 (2002) 99–115.
- [14] R. Martinez, L. Chacon-Garcia, Curr. Med. Chem. 12 (2005) 127–151.
- [15] M.H. David-Cordonnier, M.P. Hildebrand, B. Baldeyrou, A. Lansiaux, C. Keuser, K. Benzschawel, T. Lemster, U. Pindur, Eur. J. Med. Chem. 42 (2007) 752–771.
- [16] C. Keuser, U. Pindur, Pharmazie 4 (2006) 261–268.
- [17] U. Pindur, M. Jansen, T. Lemster, Curr. Med. Chem. 12 (2005) 2805–2847.
- [18] C. Hotzel, A. Marotto, U. Pindur, Eur. J. Med. Chem. 36 (2003) 189–197.
- [19] U. Pindur, T. Lemster, Recent Res. Dev. Org. Bioorg. Chem. 5 (2002) 99–115.
- [20] C. Perlick, Dissertation: 2,3-Divinyl- und 2-Aryl-3-vinylindole als Bausteine zu Carbazolen und Versuche zur photochemischen und Ultraschall-induzierten 1,6-Elektrocyclisierung, 2003.
- [21] National Cancer Institute (NCI). Bethesda. <http://dtp.nci.nih.gov>.
- [22] C.H. Spink, S.E. Wellman, Methods Enzymol. 340 (2001) 193–211.
- [23] Muth, et al., J. Heterocycl. Chem. 9 (1972) 1299.
- [24] Zhaiwei Lin, Pankaja Kadaba, Heterocycl. Commun. 8 (2002) 565–568.
- [25] A.Y. Hassan, M.M. Ghorab, O.M. Nassar, Phosphorus, Sulfur Silicon Relat. Elem. 134 (1998) 77–86.
- [26] K.B. Prasad, G.A. Swan, J. Chem. Soc. (1958) 2024–2038.
- [27] H.B. Shivarama, A. Sarvottam, J. Ind. Chem. Soc. 51 (1974) 965–966.
- [28] M. Somei, S. Sayama, K. Naka, F. Yamada, Heterocycles 27 (1988) 1585–1587.
- [29] I. Fernandez, C. Galvez, L. Urpi, An. Quim. 87 (1991) 936–939.
- [30] C. Bailly, M.J. Waring, J. Biomol. Struct. Dyn. 12 (1995) 869–898.